


RESEARCH

Open Access



Tie2-expressing monocytes/macrophages promote angiogenesis in chronically ischaemic brain tissue

Chuyang Tai^{1†}, Cong Ling^{1†}, Yang Yang^{2†}, Baoyu Zhang¹, Jun Sun¹, Ni Mo¹, Tao Sun¹, Lixin Huang¹, Cilan Yao¹, Hui Wang^{1*} and Chuan Chen^{1*} 

Abstract

Background Over half of patients with chronically ischaemic cerebrovascular disease (CICD) exhibit poor revascularization potential. Tie2-expressing monocytes/macrophages (TEMs) have been reported to promote angiogenesis in tumour tissue; however, whether TEMs promote angiogenesis in chronically ischaemic brain tissue (CIBT) and the regulatory mechanism through which TEMs are recruited to CIBT remain unclear.

Methods We first analysed the proportion of TEMs in blood from the internal jugular veins (IJVs) of CICD patients and then isolated TEMs for coculture with human umbilical vein endothelial cells (HUVECs) and for intraventricular injection into nude mice to explore the proangiogenic effects of TEMs in CIBT. Then, molecular biology experiments were performed to verify the upstream regulatory mechanism of the ANGPT2-Tie2 axis, and cell transfection experiments were conducted to confirm the regulatory effects of the detected pathway on Tie2 receptors on the endothelial cell surface. Additionally, a 2-vessel occlusion plus encephalomyosynangiosis rat model was established to confirm the recruitment mechanism of TEMs in CIBT and their ability to improve cerebral blood perfusion (CBP) and cognitive function.

Results The proportion of TEMs from the IJV blood of CICD patients significantly increased, especially in patients who exhibited Matsushima Grade-A revascularization. The viability of HUVECs cocultured with TEMs was significantly increased, and CBP and the expression of CD31 in the CIBT of nude mice treated with TEMs were significantly increased. The above increases were positively correlated with the concentration of TEMs used for coculture and intraventricular injection. Moreover, molecular biology experiments indicated that miR-126-5p can directly bind to the 3'UTR of TRPS1 mRNA and that TRPS1 can directly bind to the promoter of Angpt2. HUVECs transfected with miR-126-5p mimics presented significantly decreased TRPS1 expression, a reduced pTie2/Tie2 ratio, increased ANGPT2 expression, and increased cell viability. Finally, significantly increased TEMs infiltration, downregulated TRPS1 expression, and upregulated ANGPT2, CD31, VEGFA, and IGF1 expression were detected in the CIBT of the rats transfected with the miR-126-5p agomir, accompanied by significant improvements in CBP and cognitive function.

[†]Chuyang Tai, Cong Ling, Yang Yang contributed equally to this work.

*Correspondence:

Hui Wang
doctorwangh@163.com
Chuan Chen
chenchn6@mail.sysu.edu.cn

Full list of author information is available at the end of the article



© The Author(s) 2025. **Open Access** This article is licensed under a Creative Commons Attribution-NonCommercial-NoDerivatives 4.0 International License, which permits any non-commercial use, sharing, distribution and reproduction in any medium or format, as long as you give appropriate credit to the original author(s) and the source, provide a link to the Creative Commons licence, and indicate if you modified the licensed material. You do not have permission under this licence to share adapted material derived from this article or parts of it. The images or other third party material in this article are included in the article's Creative Commons licence, unless indicated otherwise in a credit line to the material. If material is not included in the article's Creative Commons licence and your intended use is not permitted by statutory regulation or exceeds the permitted use, you will need to obtain permission directly from the copyright holder. To view a copy of this licence, visit <http://creativecommons.org/licenses/by-nc-nd/4.0/>.

Conclusions TEMs promote angiogenesis in CIBT through a paracrine mechanism, and the recruitment of TEMs to CIBT is regulated by the miR-126-5p/TRPS1/ANGPT2 pathway.

Keywords Angiogenesis, Chronically ischaemic cerebrovascular disease, Encephalomyosynangiosis, Ischaemic stroke, Tie2-expressing monocytes/macrophages

Background

Stroke is one of the top three deadly diseases worldwide, which is most commonly induced by chronically ischaemic cerebrovascular disease (CICD) [1, 2]. However, the efficacy of revascularization surgery in more than half of CICD patients is unsatisfactory because of the lack of potential for angiogenesis [3].

In the past decade, Tie2-expressing monocytes/macrophages (TEMs) were shown to infiltrate tumour tissues and promote tumour angiogenesis through a paracrine mechanism [4–9]. Recent studies have shown that TEMs also increase the proliferation of endothelial cells (ECs) in nontumor ischaemic tissues, such as ischaemic limbs [10, 11] and brain tissue surrounding acute cerebral infarction [12]. In these ischaemic tissues, TEMs release high levels of various factors to stimulate EC proliferation [13, 14]. However, whether TEMs participate in the angiogenesis and revascularization in chronically ischaemic brain tissue (CIBT) is unknown, and the specific molecular mechanisms by which TEMs are recruited are still unclear.

MicroRNAs (miRNAs), small noncoding RNAs, suppress the expression of target genes by inhibiting transcription or destabilizing messenger RNA (mRNA) to regulate various biological processes, such as cell proliferation, differentiation, and hormone secretion [15]. Extensive evidence has revealed that miR-126-5p, which is a functional mature miRNA produced by the 5' arm of the miR-126 precursor, plays an important role in regulating EC proliferation [16–19]. Transcriptional repressor GATA binding 1 (TRPS1), a special member of the GATA transcription factor family, represses the expression of target genes by acting on the GATA regulatory element (GRE) located on the promoter or enhancer of genes [20, 21]. As an oncogene, TRPS1 is highly expressed in breast cancer [22], colon cancer [23] and other malignant tumours and has recently been shown to participate in the regulation of EC proliferation in tumour tissues [24]. In addition, bioinformatics analysis indicated that TRPS1 is a downstream factor of miR-126-5p and can act on the GRE in the *Angpt2* promoter to regulate Angiopoietin-2 (ANGPT2) expression and ANGPT2-Tie2 conjunction [25–27] (Figure S1).

On the basis of the above information, we hypothesized that TEMs are recruited to CIBT via the miR-126-5p/TRPS1/ANGPT2 pathway and promote EC proliferation

and angiogenesis in CIBT. In this study, TEMs were cocultured with human umbilical vein endothelial cells (HUVECs) under hypoxia and injected into the lateral ventricles of nude mice subjected to internal carotid artery occlusion (ICAO) plus encephalomyosynangiosis (EMS) procedures to verify the ability of TEMs to promote EC proliferation and angiogenesis in CIBT. Furthermore, the recruitment mechanism was explored both by in vitro experiments with transfected HUVECs and molecular biology experiments, including dual luciferase reporter (DLR), RNA immunoprecipitation (RIP) and chromatin immunoprecipitation (ChIP) assays, and by in vivo experiments with Sprague–Dawley (SD) rats subjected to 2-vessel occlusion (2VO) plus EMS model establishment combined with temporal muscle (TM) transfection and intraventricular injection. We believe our findings will help identify new therapeutic targets for increasing the efficacy of revascularization surgery and reducing the risk of stroke in CICD patients.

Materials and methods

Patients and blood samples

CICD patients who received indirect revascularization surgery were included in this study. Computed tomography perfusion (CTP) was performed on postoperative day 180. Digital subtraction angiography (DSA) was performed 2 years after surgery to assess the degree of indirect revascularization via the Matsushima classification system: Grade-A revascularization indicated that more than two-thirds of the middle cerebral artery (MCA) anastomosis-induced circulation was fulfilled, Grade-B revascularization indicated one-third to two-thirds fulfilment, and Grade-C revascularization indicated less than one-third fulfilment [28].

Blood samples from CICD patients with Matsushima Grade-A revascularization (n=10) and Matsushima Grade-C revascularization (n=10) were collected from the internal jugular vein (IJV) catheter during DSA examination, whereas blood samples from patients with intracranial aneurysms (as the control group, n=10) were collected in the same way. The exclusion criteria were as follows: (1) patients with malignancy; (2) patients with other ischaemic diseases, including cardiovascular diseases and peripheral vascular disease; and (3) patients with abnormal haemopoietic or immune function. Base-line data are provided in Table 1.

Table 1 Demographics of the patients included in this study

Characteristic	Patients with intracranial aneurysm (n = 10)	Matsushima Grade-A patients (n = 10)	Matsushima Grade-C patients (n = 10)	P value
Age (years)	51.5 ± 10.6	56.6 ± 9.0	53.9 ± 8.9	0.5633
Sex (male %)	50 (5/10)	50 (5/10)	60 (6/10)	0.8747
BMI (kg/m ²)	21.07 ± 1.61	21.90 ± 1.90	20.15 ± 1.78	0.1044
Hypertension (%)	50 (5/10)	50 (5/10)	70 (7/10)	0.5810
T2DM (%)	40 (4/10)	20 (2/10)	30 (3/10)	0.6211
Hyperlipidaemia (%)	20 (2/10)	40 (4/10)	40 (4/10)	0.5488
Smoking (%)	30 (3/10)	40 (4/10)	30 (3/10)	0.8607
Alcohol (%)	50 (5/10)	60 (6/10)	50 (5/10)	0.8747
WBC count (× 10 ⁹ /L)	7.14 ± 1.73	7.60 ± 1.55	7.97 ± 1.01	0.4604
Monocytes count (× 10 ⁹ /L)	0.27 ± 0.09	0.29 ± 0.11	0.23 ± 0.06	0.3339
Lymphocytes count (× 10 ⁹ /L)	1.96 ± 0.43	2.39 ± 0.39	2.23 ± 0.42	0.0796
Past TIAs (%)	–	40 (4/10)	50 (5/10)	1.0000
I/C MTT ratio before surgery	–	1.22 ± 0.15	1.25 ± 0.18	0.7189
mRS score before surgery				0.6210
0	–	3	4	
1	–	4	2	
2	–	3	4	

BMI: body mass index; T2DM: type 2 diabetes mellitus; WBC: white blood cell; TIA: transient ischaemic attack; I/C MTT: ipsilateral/contralateral mean transit time; mRS, modified Rankin scale. Continuous data are expressed as the means ± SDs. Data on age, BMI, WBC count, monocyte count, and lymphocyte count were analysed via one-way ANOVA; data on sex, hypertension status, T2DM status, hyperlipidaemia status, smoking status, alcohol status, and mRS score before surgery were analysed via the chi-square test; data on past TIAs status were analysed via the Fisher's exact test; data on the I/C MTT ratio before surgery were analysed via the unpaired t test. $P > 0.05$ indicated that there was no significant difference between any two of the three groups or between two groups

Quantification of TEMs in blood

Peripheral blood mononuclear cells (PBMCs) were isolated from IJV blood via human whole blood mononuclear cell separation solution (Solarbio, China). PBMCs were double-stained with APC-conjugated anti-CD14 (367117, BioLegend, USA) and PE-conjugated anti-Tie2 (10700-R116-F, Sino Biological, China), and TEMs were detected via flow cytometry (BD, USA).

Cell culture

HUVECs were purchased from American Type Culture Collection (ATCC) and cultured in Dulbecco's modified Eagle's medium (DMEM) with high glucose (Gibco, USA) supplemented with 10% foetal bovine serum (FBS; Gibco, USA) and 1% penicillin–streptomycin (Gibco, USA). The cells were routinely cultured in a humidified incubator at 37 °C with 21% O₂ and 5% CO₂. For hypoxic culture, the cells were cultured in a tri-gas incubator with 1% O₂, 94% N₂, and 5% CO₂. All experiments were conducted with HUVECs between the third and sixth passages.

Cell coculture and subgrouping

First, CD14⁺ cells were isolated from the PBMCs of Matsushima Grade-A patients via magnetic-activated cell sorting (MACS) (QuadroMACS Separator, LS

Separation columns; Miltenyi Biotec, German) using human CD14 magnetic beads (Miltenyi Biotec, German). Tie2 antibody (5 µg, ab221154, Abcam, UK) was labelled with NHS-Biotin (ThermoFisher, USA), and further labelled with Anti-Biotin MicroBeads (Miltenyi Biotec, Germany). Then, TEMs and Tie2-negative monocytes/macrophages (TNMs) were sorted from CD14⁺ cells via MACS and confirmed via flow cytometry and immunofluorescence. HUVECs (4 × 10³) were cocultured directly or indirectly with TEMs or TNMs in 24-well Transwell culture plates. The two methods of coculture had the following groups: (1) Control group,

Table 2 Subgrouping of HUVECs cocultured with TEMs or TNMs

Groups	Procedures
Control group	Cultured routinely
Hypoxia group	Cultured in a hypoxic environment
TNMs group	Hypoxia, cocultured with 1 × 10 ³ TNMs
TEMs group	Hypoxia, cocultured with 1 × 10 ³ TEMs
2 × TEMs group	Hypoxia, cocultured with 2 × 10 ³ TEMs
4 × TEMs group	Hypoxia, cocultured with 4 × 10 ³ TEMs

HUVECs: human umbilical vein endothelial cells; TEMs: Tie2-expressing monocytes/macrophages; TNMs: Tie2-negative monocytes/macrophages

(2) Hypoxia group, (3) TNMs group, (4) TEMs group, (5) 2×TEMs group, and (6) 4×TEMs group (Table 2).

Cell transfection and subgrouping

MiR-126-5p mimics, inhibitors and the corresponding negative control (NC) were purchased from GenePharma (Shanghai, China). The TRPS1 overexpression plasmid (pcDNA3.1-TRPS1), the plasmid expressing short hairpin RNA (shRNA) of TRPS1 (sh-TRPS1) and the corresponding NC were constructed by Synbio Technologies (Suzhou, China). HUVECs were transfected with Lipofectamine™ 3000 (Invitrogen, USA) according to the following groups: (1) Control group, (2) Hypoxia group, (3) Mimics NC group, (4) Mimics group, (5) Mimics+pcDNA3.1 NC group, (6) Mimics+pcDNA3.1-TRPS1 group, (7) Inhibitors NC group, (8) Inhibitors group, (9) Inhibitors+sh NC group, and (10) Inhibitors+sh-TRPS1 group (Table 3). All information on miRNAs and plasmids used for transfection is provided in the supplementary materials (Figure S2, Table S1, and Table S2).

Ethynyl deoxyuridine (EdU) assay

An EdU assay was performed to evaluate the proliferation of HUVECs cocultured with TEMs or TNMs, and the BeyoClick™ EdU Cell Promotion Kit with Alexa Fluor 555 (Beyotime, China) was used according to the manufacturer's protocol. After overnight coculture, the cells were incubated with 20 μmol/L EdU working solution for 2 h, washed with phosphate buffer solution (PBS) containing 3% bovine serum albumin (BSA; Beyotime, China), fixed and permeabilized with 4% paraformaldehyde (PFA; Beyotime, China) and 0.3% Triton X-100 (Beyotime, China) for 15 min. For direct coculture, anti-CD31 (1:1000, 28083-1-AP, Proteintech, China) and 488-conjugated goat anti-rabbit (1:2000, ab6721, Abcam, UK) antibodies

were additionally used to label the HUVECs. Finally, the cells were stained with Click reaction solution, and the cell nuclei were stained with Hoechst 33342. Images were obtained via confocal microscopy (Olympus, Japan), and the percentage of EdU-positive HUVECs indicated the extent of cell proliferation. Each experiment was performed at least three times.

Flow cytometric analysis of apoptosis

Flow cytometry was performed to evaluate the apoptosis of HUVECs cocultured with TEMs or TNMs, and an Annexin V-FITC Apoptosis Detection Kit (Beyotime, China) was used according to the manufacturer's protocol. After overnight coculture, the cells were collected in flow cytometry tubes, washed three times with cold PBS, and resuspended in 195 μL of binding buffer. The cell suspension was subsequently mixed with 5 μL of Annexin V-FITC staining solution and 10 μL of propidium iodide staining solution at room temperature in a dark room for 15 min. For direct coculture, anti-CD31 (10148-MM13-A, Sino Biological, China) was also used to label the HUVECs. The apoptosis rate of HUVECs was evaluated via flow cytometry (BD, USA) within 1 h. Each experiment was performed at least three times.

Tube formation assay

A tube formation assay was performed to evaluate the ability of HUVECs to form tubule-like structures. HUVECs (1×10^4) from each group were inoculated into each well of a 96-well plate containing 50 μL of Matrigel (Corning, USA). After 24 h of incubation, tube formation was observed via an inverted phase-contrast microscope (Olympus, Japan). Images were analysed via ImageJ software (National Institutes of Health, USA), and the extent of tubule formation was quantified by counting the total length, number of branches, and number of nodes in five

Table 3 Subgrouping of HUVECs transfected with miRNAs and plasmids

Groups	Procedures
Control group	Cultured routinely
Hypoxia group	Cultured in a hypoxic environment
Mimics NC group	Hypoxia, transfected with miRNA mimics NC
Mimics group	Hypoxia, transfected with has-miR-126-5p mimics
Mimics+pcDNA3.1 NC group	Hypoxia, cotransfected with has-miR-126-5p mimics and pcDNA3.1 NC
Mimics+pcDNA3.1-TRPS1 group	Hypoxia, cotransfected with has-miR-126-5p mimics and pcDNA3.1-TRPS1
Inhibitors NC group	Hypoxia, transfected with miRNA inhibitors NC
Inhibitors group	Hypoxia, transfected with hsa-miR-126-5p inhibitors
Inhibitors+sh NC group	Hypoxia, cotransfected with hsa-miR-126-5p inhibitors and shRNA NC
Inhibitors+sh-TRPS1 group	Hypoxia, cotransfected with hsa-miR-126-5p inhibitors and shRNA-TRPS1-2 (validated by qRT-PCR, Fig S2)

HUVECs: human umbilical vein endothelial cells; NC, negative control

random fields of view ($\times 100$). Each experiment was performed at least three times.

Scratch wound assay

A scratch wound assay was performed to evaluate the migration ability of HUVECs. The cell culture medium was replaced with serum-free medium. Then, HUVECs from each group of 6-well plates were scratched with a 200- μ L micropipette tip and washed with PBS. After 24 h of incubation, the degree of wound closure was observed via microscopy. The wound width was measured via ImageJ software, and the migration ability was evaluated by the percentage of wound closure. Each experiment was performed at least three times.

Transwell migration assay

Transwell migration assays were also performed to evaluate the migration of HUVECs. HUVECs (1×10^4) from each group were resuspended in serum-free medium and inoculated into the upper layer of the Transwell chamber, while complete medium was added to the lower layer. After 24 h of incubation, the cells that had migrated to the lower layer were stained with crystal violet (Beyotime, China) and observed under a microscope. The number of stained cells located in the lower layer was determined via ImageJ software, which indicates the degree of HUVECs migration. Each experiment was performed at least three times.

Methylthiazolyldiphenyl-tetrazolium bromide (MTT) proliferation assay

An MTT proliferation assay was performed to evaluate the viability of HUVECs. HUVECs (1×10^4) from each group were inoculated into 96-well plates. After adhesion, the cells were incubated with 100 μ L of MTT solution (5 mg/mL; Beyotime, China) for 4 h at 37 °C. The supernatant was subsequently removed, and 200 μ L of dimethyl sulfoxide (DMSO; Beyotime, China) was added to each well. The optical density (OD) values at a wavelength of 490 nm were measured via a multifunctional enzyme-linked immunosorbent assay (ELISA) reader (BioTek, USA) at 24 h and 48 h, which indicated the viability of the HUVECs. Each experiment was performed at least three times.

Dual-luciferase reporter (DLR) assay

A DLR assay was performed to verify the direct regulatory relationship between miR-126-5p and TRPS1. According to the potential binding sites of miR-126-5p on TRPS1 mRNA 3'UTR predicted via miRDB database [25] (Figure S1C), four plasmids containing the TRPS1 3'UTR-wt and five plasmids containing the TRPS1 3'UTR-mut were constructed via the pGL basic

vector (Promega, USA) (Fig. 6A, Table S2). HEK-293 T cells (1×10^3) were seeded in 96-well plates 24 h before transfection, and 0.1 μ g of plasmid, 0.01 μ g of pGL-TK and 50 nM miR-126-5p mimics (GenePharma, China) or their NC were cotransfected with LipofectamineTM 3000 (Invitrogen, USA). After 48 h of transfection, the luciferase assay reagent II (Promega, USA) was used to measure firefly luciferase activity, the Stop & Glo Reagent (Promega, USA) was used to measure Renilla luciferase activity, and luciferase activity was calculated via a multifunctional ELISA reader (BioTek, USA). Relative luciferase activity was defined as the ratio of firefly luciferase activity to Renilla luciferase activity. Each experiment was performed at least three times. All sequences of miRNAs, TRPS1 3'UTR-wt and mut are provided in the Table S1 and Table S3.

RNA immunoprecipitation (RIP) assay

A RIP assay was also performed to verify the direct regulatory relationship between miR-126-5p and TRPS1, and the Imprint[®] RNA Immunoprecipitation Kit (Sigma, German) was used according to the manufacturer's protocol. HUVECs were harvested and lysed with complete RIP lysis buffer. The cells were subsequently incubated with anti-AGO2 (5 μ g, 67934-1-Ig, Proteintech, China) or anti-IgG (5 μ g, 30000-0-AP, Proteintech, China) antibodies combined with ProteinA/G magnetic beads overnight at 4 °C. The precipitate was extracted via a magnetic rack, and RNA was extracted via TRIzol (Sigma, Germany). The RNA fraction was reverse transcribed and analysed via qRT-PCR. All information on the primers is provided in the Table S4.

Chromatin immunoprecipitation (ChIP) assay

A ChIP assay was performed to verify the direct regulatory relationship between TRPS1 and ANGPT2. HUVECs were fixed with 1% formaldehyde and lysed with SDS lysis buffer (Beyotime, China). The cells were subsequently sonicated, and protein-DNA crosslinks were removed by heating at 65 °C. After incubation with ProteinA + G Agarose/Salmon Sperm DNA (Sigma, German), the cells were incubated with anti-TRPS1 (5 μ g, 21938-1-AP, Proteintech, China) and anti-IgG (5 μ g, 30000-0-AP, Proteintech, China) antibodies overnight at 4 °C. After the precipitate was washed, the DNA was purified and concentrated. Finally, the DNA fraction was analysed via qRT-PCR. The information on the primer is provided in the Table S4.

Animals

Adult BALB/c nude mice (male, 20–25 g, 42 in total, $n=6$ mice/group, three for western blotting and three for immunofluorescence) and adult SD rats (male,

260–280 g, 81 in total, $n=9$ rats/group, three for western blotting, three for immunofluorescence, and three for electron microscopy) were purchased from ZhuHai Bestest Biotechnology Co., Ltd. (Guangdong, China), and housed under specific pathogen-free (SPF)-grade conditions (temperature $22\text{ }^{\circ}\text{C}\pm 2\text{ }^{\circ}\text{C}$, humidity $55\%\pm 5\%$, 12 h light/dark cycle). The animals were allowed to adapt to the environment for 1 week before the experiment.

Nude mice were subjected to ICAO modelling and received different treatments. The rats were subjected to 2VO plus EMS modelling. All the animals were randomly divided into different groups, as shown in Tables 4 and 5.

Nude mouse model of unilateral chronic cerebral ischaemia

A chronic cerebral ischaemia model in nude mice was established via unilateral ICAO [29], which effectively reduced unilateral CBP in nude mice (Figure S4A–B). The mouse was anaesthetized with isoflurane (3% for induction, 1.5% for maintenance, 0.6 L/min oxygen flow; RWD, China) and fixed on an electric blanket, and its temperature was monitored and maintained at $37\text{ }^{\circ}\text{C}$. After an incision was made in the middle of the neck, the right

internal carotid artery (ICA) was carefully separated and ligated with 7–0 silk sutures. Be careful to avoid damaging the vagus nerve. Finally, the skin was sutured (Fig. 1A, B). Successful ICAO model establishment was confirmed by magnetic resonance imaging (MRI) as follows: (1) no large infarct foci on the T2WI sequence 1 day after the ICAO procedure and (2) an arterial spin labelling (ASL) sequence showing that the cerebral blood flow (CBF) value on the modelling side was 40% lower than that on the contralateral side (Fig. 1C, D, Figure S4C).

Cell transplantation

TEMs or TNMs were transplanted into the cerebrospinal fluid through intraventricular injection. After the ICAO procedure, the mouse was immediately placed in a stereotaxic apparatus (RWD, China). In accordance with the map of mouse brain regions, a hole was drilled on the skull, and a microinjector (Hamilton, USA) was implanted into the right lateral ventricle (mouse coordinates for the microinjector tip, from bregma: ML = 1 mm, AP = 0.5 mm, DV = 2.4 mm). The cells were resuspended in serum-free Roswell Park Memorial Institute (RPMI) 1640 medium, the cell suspension was injected into the

Table 4 Subgrouping of nude mice

Groups (n = 6)	Procedures
ICAO group	ICAO
ICAO + EMS group	ICAO + EMS
RPMI 1640 group	ICAO + EMS with serum-free RPMI 1640 medium injected into the lateral ventricle as a vehicle control group
TNMs group	ICAO + EMS with 1×10^5 TNMs injected into the lateral ventricle
TEMs group	ICAO + EMS with 1×10^5 TEMs injected into the lateral ventricle
2×TEMs group	ICAO + EMS with 2×10^5 TEMs injected into the lateral ventricle
4×TEMs group	ICAO + EMS with 4×10^5 TEMs injected into the lateral ventricle

ICAO: internal carotid artery occlusion; EMS: encephalomyosynangiosis; RPMI: Roswell Park Memorial Institute; TNMs: Tie2-negative monocytes/macrophages; TEMs: Tie2-expressing monocytes/macrophages

Table 5 Subgrouping of rats

Groups (n = 9)	Procedures
Control group	2VO + EMS
Agomir NC group	2VO + EMS with miRNA agomir NC transfected in TM tissue
Agomir group	2VO + EMS with rno-mir-126a-5p agomir transfected in TM tissue
Agomir + LV-sh NC group	2VO + EMS with rno-mir-126a-5p agomir transfected in TM tissue and LV-shRNA NC injected into the lateral ventricle
Agomir + LV-sh-ANGPT2 group	2VO + EMS with rno-mir-126a-5p agomir transfected in TM tissue and LV-shRNA-ANGPT2-2 (validated by qRT-PCR, Fig S3) injected into the lateral ventricle
Antagomir NC group	2VO + EMS with miRNA antagomir NC transfected in TM tissue
Antagomir group	2VO + EMS with rno-mir-126a-5p antagomir transfected in TM tissue
Antagomir + LV NC group	2VO + EMS with rno-mir-126a-5p antagomir transfected in TM tissue and LV NC injected into the lateral ventricle
Antagomir + LV-ANGPT2 group	2VO + EMS with rno-mir-126a-5p antagomir transfected in TM tissue and LV-ANGPT2 injected into the lateral ventricle

2VO: 2-vessel occlusion; EMS: encephalomyosynangiosis; TM: temporal muscle; NC: negative control; LV: lentivirus

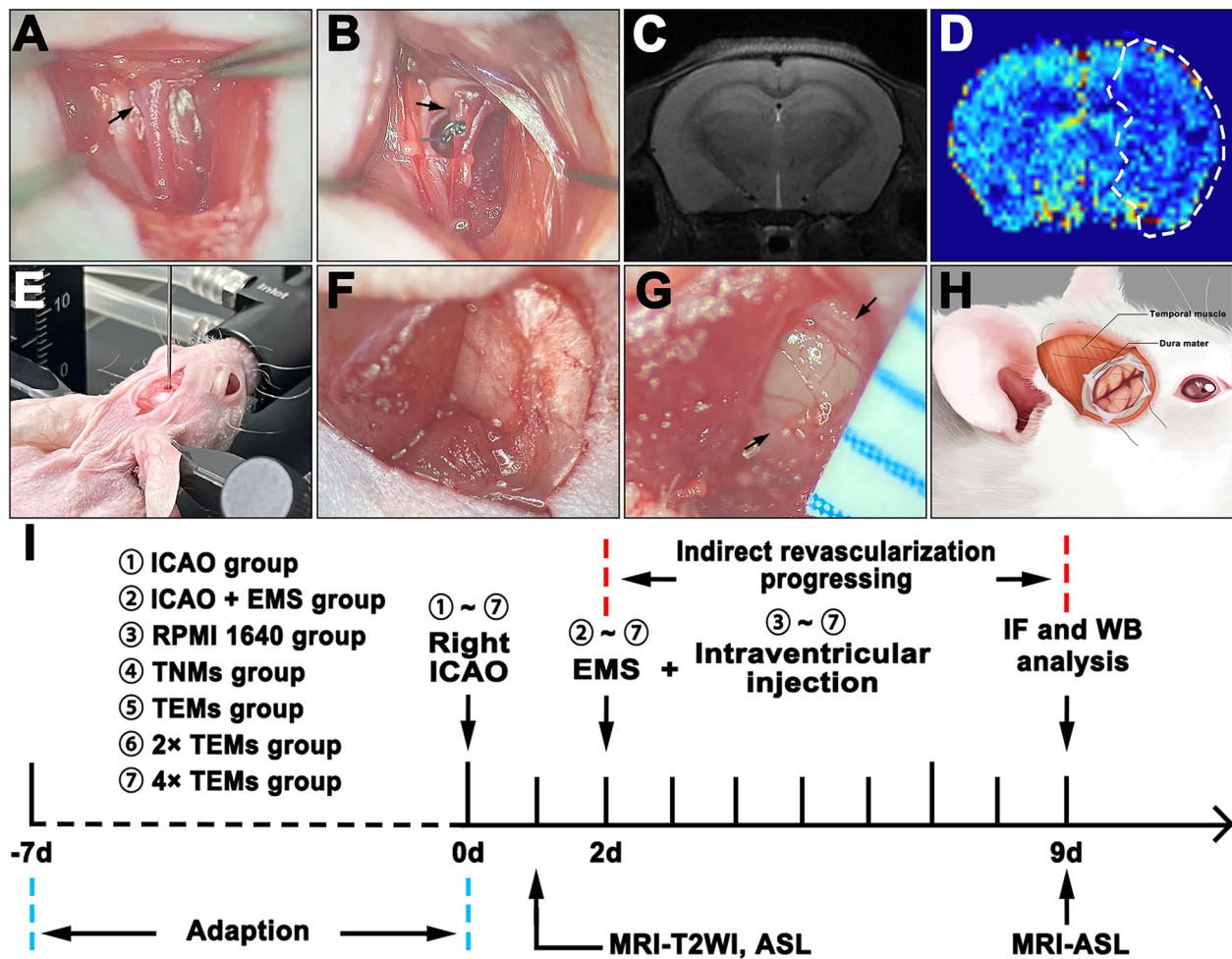


Fig. 1 Procedures for establishing the ICAO + EMS model in nude mice. **A, B** Procedures for ligating the right ICA (the black arrow indicates the right ICA). **C** Representative MRI-T2WI film showing no infarction after the ICAO procedure. **D** Representative MRI-ASL film showing a decrease in the CBP on the modelling side after the ICAO procedure (the white dashed line indicates the range of CBP decrease). **E** The procedure for intraventricular injection. Representative images showing the procedures for EMS surgery, including **F** reflection of the skin and TM tissue from the skull and **G** opening of the DM (the black arrow indicates the opened DM and arachnoid membrane). **H** Schematic diagram of EMS surgery. **I** Experimental schedule. ASL: arterial spin labelling; CBP: cerebral blood perfusion; DM: dura mater; EMS: encephalomyosynangiosis; ICA: internal carotid artery; ICAO: internal carotid artery occlusion; IF: immunofluorescence; MRI: magnetic resonance imaging; TM: temporal muscle; T2WI: T2-weighted imaging; WB: western blotting

right lateral ventricle (1 μ L, 0.1 μ L/min), and the micro-injector was slowly removed after being left for 10 min (Fig. 1E).

EMS surgery for nude mice

Each mouse was anaesthetized and maintained as described above. An incision of the skin and TM was then made, and a piece of skull (2 mm diameter) was ground away from the temporoparietal region via an electric drill. The dura mater (DM) and arachnoid membrane were carefully opened via forceps and a 1 mL syringe needle. The TM and DM were sutured together, and finally, the skin was sutured (Fig. 1F–H).

Rat model of chronic cerebral ischaemia plus revascularization surgery

A 2VO + EMS model was established to simulate chronic cerebral ischaemia plus revascularization surgery in rats. The anaesthesia and incision procedures used for the 2VO modelling were performed in a similar way as those used for ICAO modelling. The left common carotid artery (CCA) was dissected and ligated with two 5–0 silk sutures, and the right CCA was ligated 7 days later (Fig. 2A, B). Successful 2VO model establishment was confirmed by the following: (1) postoperative CBF value less than 40% of the baseline value detected by a laser Doppler blood flow metre and (2) no large infarct foci on

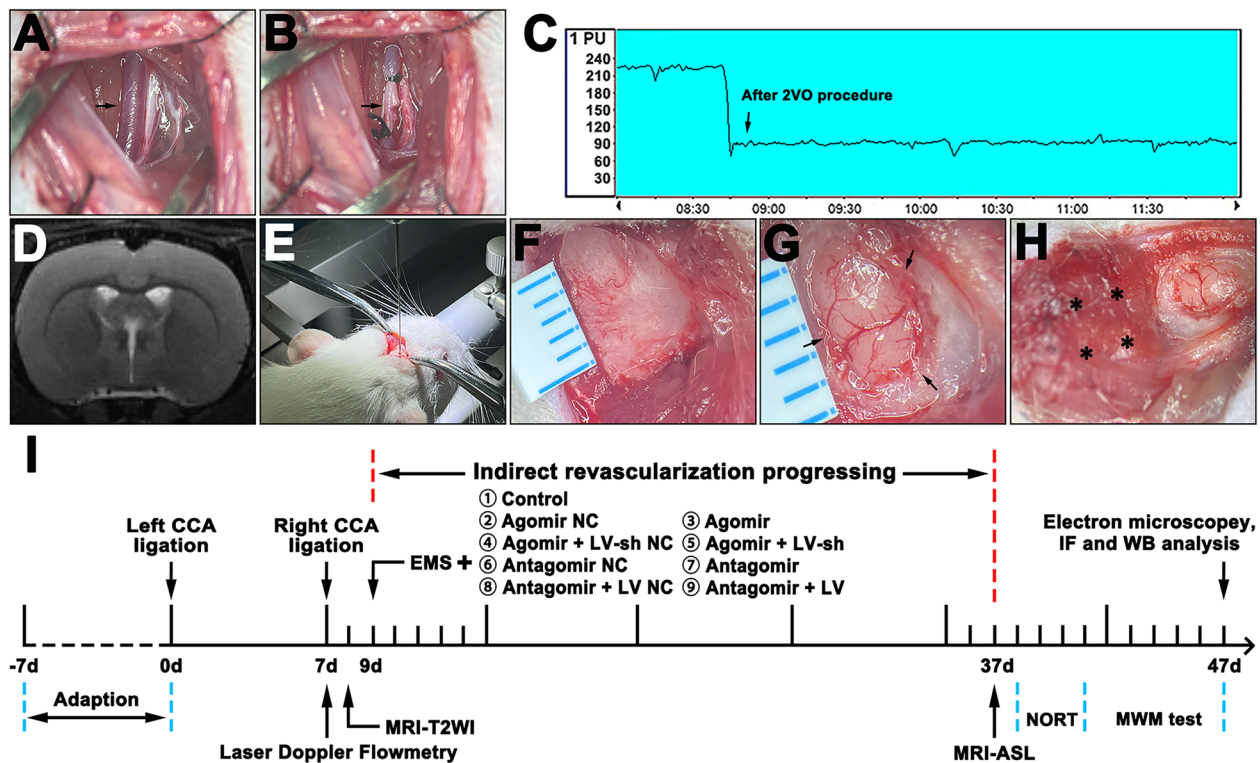


Fig. 2 Procedures for establishing the 2VO + EMS model in SD rats. **A, B** Procedures for ligating the CCA (the black arrow indicates the left CCA). **C** Representative laser doppler flow metre confirming the decrease in the CBF value during the 2VO procedure. **D** MRI-T2WI image showing no infarction after the 2VO procedure. **E** The procedure of intraventricular injection. Representative images showing the procedures of EMS surgery, including **F** reflection of the skin and TM from the skull, **G** opening of the DM (the black arrow indicates the opened DM and arachnoid membrane), and **H** displaying the four sites on TM tissue for miRNA transfection. **I** Experimental schedule. CBF: cerebral blood flow; CCA: common carotid artery; DM: dura mater; EMS: encephalomyosynangiosis; IF: immunofluorescence; MRI: magnetic resonance imaging; MWM: Morris water maze; NORT: novel object recognition test; TM: temporal muscle; T2WI: T2-weighted imaging; WB: western blotting; 2VO: 2-vessel occlusion

the T2WI sequence of the MRI 1 day after the 2VO procedure (Fig. 2C, D). Finally, EMS surgery was performed in a similar way as the nude mice received (Fig. 2E, G).

Lentivirus infection and miRNA transfection

The lentivirus expressing ANGPT2 (LV-ANGPT2) and its corresponding shRNA (LV-sh-ANGPT2) were designed and packaged by GenePharma (Shanghai, China). Lentivirus infection was performed via intraventricular injection (rat coordinates for the microinjector tip, from bregma: ML=1.5 mm, AP=1 mm, DV=3.5 mm) just before EMS surgery. The lentivirus (1×10^8 TU/mL) was injected into the right lateral ventricle (10 μ L, 1 μ L/min), and the microinjector was slowly removed after being left for 10 min (Fig. 2E). The miR-126-5p agomir, antagomir and NC were purchased from GenePharma (Shanghai, China). The miRNA suspension [20 μ g of miRNA in 10 μ L of normal saline (NS)] was equally divided into four parts and injected into four sites of the TM tissue via a microinjector during EMS surgery (Fig. 2H). All information on the miRNAs and lentiviruses used for the animal

experiments is provided in the supplementary materials (Figure S3, Table S1, and Table S2).

MRI

The ASL sequence of MRI was used to evaluate the CBP of the animals in each group. The animals were scanned via 7.0 T MRI (PharmaScan 70/16 US with ParaVision version 6.0.1 system; Bruker, USA). The animals were anaesthetized with isoflurane, and respiration was monitored with a small animal monitoring system (Model 1030; SA Instruments, Inc., USA) and controlled at 50–60 breaths/min. The best slice for brain muscle fitting was confirmed on the T2WI image, and then, ASL sequence scanning was performed on the selected slice. The cerebral cortex in close contact with the TM after EMS surgery (within a 1 mm range) and the cortex in the symmetrical position of the opposite hemisphere were selected as the regions of interest (ROIs). The mean CBF value (mL/100 g min) of each ROI was calculated with ParaVision software, and the improvement in CBP after EMS surgery was evaluated by the perfusion ratio of the

mean CBF value on the EMS side to that on the non-EMS side.

The T2WI parameters were set as follows: repetition time (TR)=3500 ms; echo time (TE)=48 ms; average=2; image size=256×256; field of view (FOV)=35×35 mm²; slice thickness=0.7 mm; and scan time=2 min 27 s.

The ASL parameters were set as follows: TR=10,000 ms; TE=4.95 ms; inversion times (TI)=30, 100, 200, 300, 400, 500, 800, 1200, 3000, and 5000 ms; image size=96×96; FOV=40×40 mm²; slice thickness=1.2 mm; and scan time=10 min.

Behavioural testing

The novel object recognition test (NORT) and Morris water maze (MWM) were used to evaluate the cognitive function of the rats. All tests were performed between 10:00 and 15:00 by experimenters who were blinded to the groupings of the rats. The rats were kept in the behavioural laboratory 24 h before and during the experiment to eliminate the influence of the test environment. Both the NORT and MWM test results were analysed via SMART version 3.0 software (Panlab, Spain).

NORT

The first day was the adaptation period, and the rats could freely explore the open field box (80 cm×80 cm×60 cm) without objects for 10 min. The second day was the familiar period. Two identical objects were placed in the test box, and the rats were allowed to explore for 5 min. The third day was the test period, one of the familiar objects was replaced with a novel object, and the rats were allowed to explore for 5 min. The time the rats took to recognize each object was recorded. The recognition of an object was defined as pointing the nose at the object at a distance of less than 1 cm or touching it. Each time, the rat was placed with its back facing the objects. The odours on the test box and objects were removed with 75% alcohol before each experiment.

MWM

A circular pool (diameter 180 cm, height 60 cm) was filled with water and maintained at 22 °C±2 °C. Four visual cues were placed in the four quadrants of the pool. An escape platform was submerged 1 cm below the water surface in the centre of the third quadrant, and edible melanin was added to the water to make the platform invisible. The first five days were the learning period, and the rats were released from the four quadrants facing the wall in random order. The rats needed to find the underwater platform within 60 s, and the escape latency and swimming route were recorded. If a rat did not find the platform, it was guided to the platform, and its escape latency was recorded as 60 s. Each rat was allowed to stay

on the escape platform for 10 s regardless of whether the platform was found. The sixth day was the test day, the platform was removed, the rats were placed in the opposite quadrant from the target quadrant, and the escape latency, time spent in the target quadrant, number of platform crossings, and swimming route were recorded.

Brain tissue collection

The animals were anaesthetized with Ulatan (20%, 1000 mg/kg), and the abdominal and thoracic cavities were incised to expose the liver and heart. The right atrial appendage was cut open, and NS was continuously injected into the left ventricle until the liver turned white. The skull was removed, and the brain tissue was collected. The samples used for immunofluorescence and electron microscopy were fixed with 4% PFA (Beyotime, China) and 2.5% glutaraldehyde (Beyotime, China), while the samples used for western blotting were stored at −80 °C.

Transmission electron microscopy

Transmission electron microscopy was performed to observe the vacuoles and tight junctions (TJs) in ECs. The brain tissues were routinely cut into ultrathin resin sections. Images were subsequently obtained at 80 kV via a JEM-1400 transmission electron microscope (JEOL, Japan). The number of vacuoles to the circumference of the vascular endothelium and the proportion of abnormal TJs were calculated to evaluate the improvement in hypoxia in brain tissues.

Scanning electron microscopy

Scanning electron microscopy was performed to observe the morphology of the pericytes. Increasing grades of alcohol were used for dehydration, and brain tissues were critical point-dried and coated with gold. Images were subsequently obtained via an SU8100 scanning electron microscope (Hitachi, Japan).

Immunofluorescence

Immunofluorescence was performed to determine the effects of TEMs and the miR-126-5p/TRPS1/ANGPT2 pathway. The brain tissue samples were routinely made into paraffin sections. After deparaffinization and rehydration, the brain tissue paraffin sections were repaired with EDTA repair solution (Beyotime, China) in a boiling water bath for 30 min, permeabilized and blocked with 0.3% Triton X-100 (Beyotime, China) and 5% BSA (Beyotime, China). Then, the slices were incubated with primary antibodies against CD31 (1:250, sc-20071, Santa Cruz, USA), ANGPT2 (1:250, Sc-74403, Santa Cruz, USA), Tie2 (1:250, DF7500, Affinity, USA), VEGFA (1:100, orb153328, Biorbyt, UK) and IGF1 (1:100,

ab106836, Abcam, UK) in PBS containing 0.2% Tween-20 (PBST) diluted overnight at 4 °C. After being washed with PBST, the slices were incubated with 488-conjugated goat anti-rabbit (1:2000, ab150077, Abcam, UK), 594-conjugated goat anti-mouse (1:2000, ab150116, Abcam, UK), and 647-conjugated donkey anti-goat (1:2000, ab150135, Abcam, UK) secondary antibodies at room temperature in a dark room for 2 h. The 647-conjugated CD11b antibody (0.5 µg, CL647-65229, proteintech, China) was used to directly label CD11b. After washes, the slices were sealed with mounting medium with DAPI (Abcam, UK), and fluorescence images were acquired via confocal microscopy (Olympus, Japan).

Western blotting

Western blotting was performed to determine the relative expression of proteins. Total proteins were extracted from HUVECs and brain tissues (approximately 1 mm around the EMS surgical site) via a radioimmunoprecipitation assay (RIPA; Beyotime, China) with phenylmethanesulfonyl fluoride (PMSF; Beyotime, China) and a phosphatase inhibitor cocktail (Beyotime, China). After ultrasonic crushing and high-speed centrifugation at 4 °C, protein concentrations were measured with a bicinchoninic acid (BCA) protein assay kit (Beyotime, China). Subsequently, 20 µg of protein was separated via 10% SDS-PAGE and transferred onto polyvinylidene fluoride (PVDF) transfer membranes (Millipore, USA) with a 0.45 µm pore size. After being blocked for 2 h with Tris-buffered saline (TBS) containing 5% nonfat skim milk (Beyotime, China) or BSA (Beyotime, China), the membranes were incubated with primary antibodies against TRPS1 (1:1000, 21938-1-AP, Proteintech, China), ANGPT2 (1:1000, 24613-1-AP, Proteintech, China), Tie2 (1:1000, DF7500, Affinity, USA), phospho-Tie2 (1:1000, bs-12262R, Bioss, China), CD11b (1:1000, sc-1186, Santa Cruz, USA), VEGFA (1:1000, 19003-1-AP, Proteintech, China), IGF1 (1:1000, ab106836, Abcam, UK), CD31 (1:1000, sc-20071, Santa Cruz, USA), or β -actin (1:20000, 66009-1-Ig, Proteintech, China) in TBS containing 0.2% Tween-20 (TBST) diluted overnight at 4 °C. After being washed with TBST, the membranes were incubated with HRP-conjugated goat anti-rabbit (1:10000, ab6721, Abcam, UK), HRP-conjugated goat anti-mouse (1:10000, ab6728, Abcam, UK) or HRP-conjugated rabbit anti-goat (1:10000, ab6741, Abcam, UK) secondary antibodies at room temperature for 2 h. After washes, the signals were detected via enhanced chemiluminescence (ECL) Ultra reagent (NCM Biotech, China) and a chemiluminescence system (Tanon, China). Images were analysed via ImageJ software. Each experiment was repeated at least three times.

Statistical analysis

The statistical analyses were performed via the Statistical Program for Social Science (SPSS) version 23.0 (IBM Corporation, USA) and GraphPad Prism version 9.5 (GraphPad Software, USA). Statistical analysis was performed via unpaired t test, chi-square test, Fisher's exact test, one-way analysis of variance (ANOVA) test, or two-way ANOVA test. Data from replicate experiments are represented as means \pm SDs. Statistically significant differences were indicated when $P < 0.05$.

Results

The proportion of TEMs is increased in the blood of CICD patients

We obtained IJV blood from CICD patients with Matsushima Grade-A revascularization ($n=10$), Matsushima Grade-C revascularization ($n=10$), and patients with intracranial aneurysms ($n=10$, as the control group) and isolated PBMCs from the blood. Flow cytometry revealed that the proportion of TEMs ($CD14^+/Tie2^+$) in the PBMCs of either the Matsushima Grade-A patients or the Matsushima Grade-C patients was significantly greater than that in the PBMCs of the aneurysm patients ($P < 0.0001$, $P = 0.0423$). In addition, the proportion of TEMs in the Matsushima Grade-A patients was significantly greater than that in the Matsushima Grade-C patients ($P = 0.0471$) (Fig. 3).

TEMs show angiogenic activity in vitro and in the CIBTs of nude mice

We isolated TEMs ($Tie2^+/CD14^+$) and TNMs ($Tie2^-/CD14^+$) from the PBMCs of Matsushima Grade-A patients via MACS and confirmed the expression of CD14 and Tie2 via flow cytometry and immunofluorescence (Fig. 4A, B). Then, we cocultured them with HUVECs via direct and indirect cocultures (Fig. 4C). EdU assays and flow cytometric apoptosis analysis revealed that the percentages of EdU-positive HUVECs in the TEMs groups was significantly greater than those in the hypoxia groups ($P = 0.0403$ in direct coculture and $P = 0.0415$ in indirect coculture) and the apoptosis rates in the TEMs groups was significantly lower than those in the hypoxia groups ($P < 0.0001$ in direct coculture and $P < 0.0001$ in indirect coculture) in both coculture methods, whereas TNMs groups did not show significant difference ($P = 0.9972$, $P > 0.9999$, $P > 0.9999$, $P = 0.9982$). There was no significant difference in the proliferation or apoptosis of HUVECs between the direct and indirect cocultures with TEMs (Fig. 4D–G). Tube formation assays revealed that the total length, number of branches, and number of nodes in the TEMs group were significantly greater than those in the hypoxia group

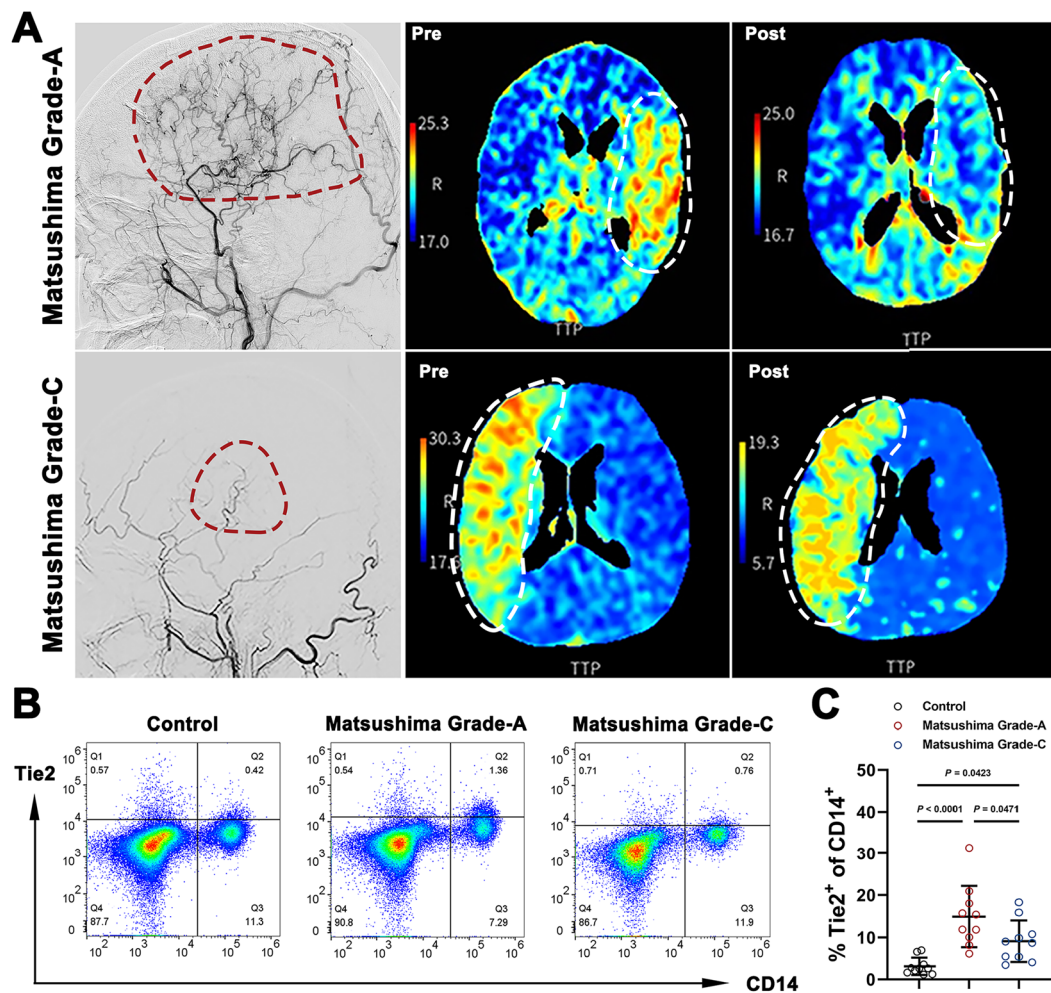


Fig. 3 Changes in TEMs from the IJV blood of CICD patients. **A** Representative DSA and CTP images showing angiogenesis and CBP improvement in CICD patients with Matsushima Grade-A revascularization and Matsushima Grade-C revascularization. **B** Representative flow cytometric dot plots of TEMs from the IJV blood of patients with intracranial aneurysms (control group), CICD patients with Matsushima Grade-A revascularization and CICD patients with Matsushima Grade-C revascularization. **C** Scatter plot showing the differences among the three groups (n=10, one-way ANOVA and Tukey's multiple comparisons test). The error bars represent the \pm SDs. CBP: cerebral blood perfusion; CICD: chronically ischaemic cerebrovascular disease; CTP: computed tomography perfusion; DSA: digital subtraction angiography; IJV: internal jugular vein; TEMs: Tie2-expressing monocytes/macrophages

($P=0.0011$, $P=0.0008$, $P=0.0300$), whereas the total length, number of branches, and number of nodes in the TNMs group did not significantly differ from those in the hypoxia group ($P=0.3517$, $P=0.7953$, $P=0.7570$) (Fig. 4H, I). In addition, these effects significantly increased with increasing concentrations of cocultured TEMs.

We next established an ICAO+EMS model in BALB/c nude mice and injected TEMs/TNMs into their lateral ventricles. The MRI-ASL films revealed that the perfusion ratios of the mean CBF value on the EMS side to the non-EMS side were significantly

greater in the TEMs group than in the ICAO+EMS group ($P=0.0222$), whereas the TNMs group did not show a significant difference ($P=0.9319$) (Fig. 5A, B). Western blotting and immunofluorescence revealed that the expression level of CD31 in the brain tissue around the EMS site in the mice treated with TEMs was significantly greater than that in the ICAO+EMS group ($P<0.0001$, $P=0.0228$), whereas the TNM group did not show a significant difference ($P=0.9989$, $P=0.9981$) (Fig. 5C–F). In addition, a greater dose of TEMs for intraventricular injection was associated with higher perfusion ratios and CD31 expression.

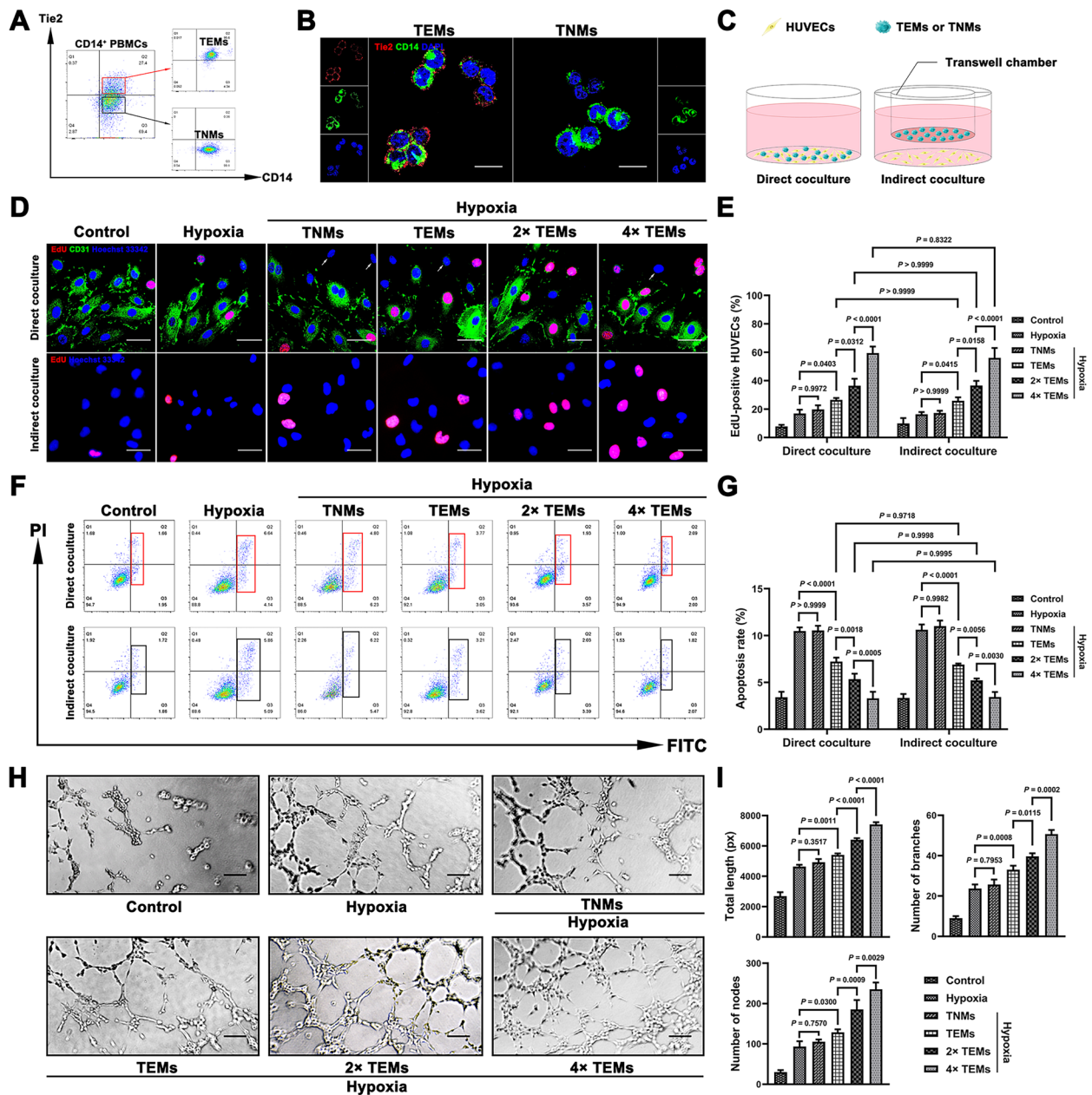


Fig. 4 The results of cell coculture showing the pro-angiogenesis effect of TEMs. **A** Representative flow cytometric dot plot identifying CD14⁺ PBMCs, TEMs and TNMs. **B** Representative immunofluorescence images identifying TEMs (Tie2⁺/CD14⁺) and TNMs (Tie2⁻/CD14⁺). Bar = 20 μ m. **C** Schematic diagram of the two methods for coculture. **D** Representative confocal images showing the results of the EdU assay for each group. Bar = 50 μ m. **E** The results were quantified by the percentage of EdU-positive HUVECs per field (n = 3, two-way ANOVA and Šidák's multiple comparisons test). **F** Representative flow cytometric dot plot showing the results of the apoptosis assay for each group. **G** Column chart showing the degree of apoptosis in each group (n = 3, two-way ANOVA and Šidák's multiple comparisons test). **H** Representative fields showing the results of the tube formation assays for each group. Bar = 200 μ m. The results were quantified by **I** the total length, number of branches, and number of nodes (n = 3, one-way ANOVA and Tukey's multiple comparisons test). The error bars represent the \pm SDs. EdU: ethynyl deoxyuridine; HUVECs: human umbilical vein endothelial cells; PBMCs: peripheral blood mononuclear cells; TEMs: Tie2-expressing monocytes/macrophages; TNMs: Tie2-negative monocytes/macrophages

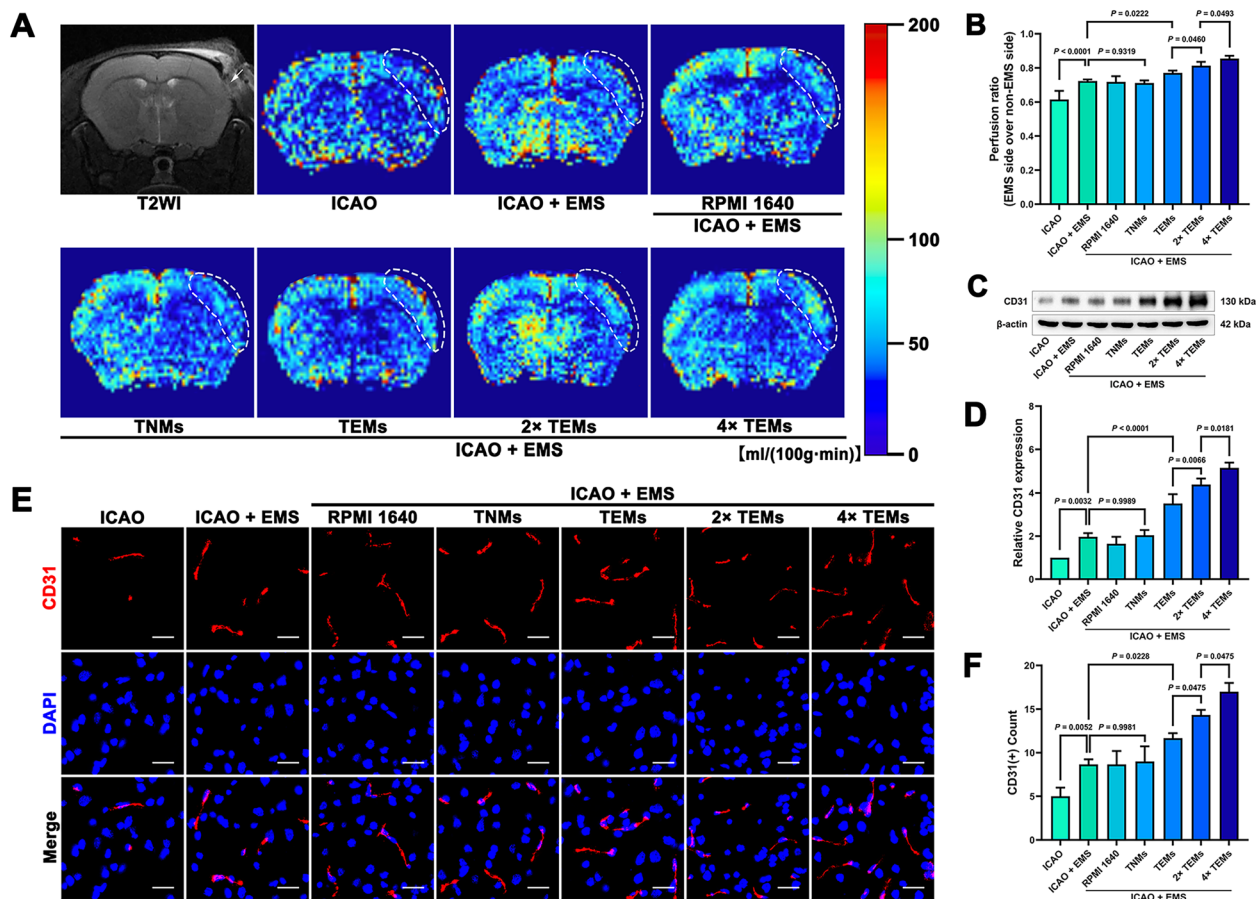


Fig. 5 Results of MIR-ASL scanning and CD31 expression detection in the brains of nude mice. **A** Representative MRI-T2WI film showing the EMS surgical site (white arrow indicates the EMS) and MIR-ASL films showing differences in CBP between the various groups (white dashed lines indicate ROIs under the EMS surgical sites). **B** Column chart showing the perfusion ratios (EMS sides over non-EMS sides) of each group (n=6, one-way ANOVA and Šidák's multiple comparisons test). **C** Representative western blot showing the relative expression of CD31 in the CIBT adjacent to the TM tissue in each group (normalized to β-actin expression). **D** Densitometric analyses of the relative expression of CD31 (n=3, one-way ANOVA and Šidák's multiple comparisons test). **E** Representative confocal images showing the expression of CD31 in the CIBT in each group. Bar = 20 μm. **F** Column chart showing the counts of CD31⁺ cells in each group (n=3, one-way ANOVA and Šidák's multiple comparisons test). The error bars represent the ± SDs. ASL: arterial spin labelling; CBP: cerebral blood perfusion; CIBT: chronically ischaemic brain tissue; EMS: encephalomyosynangiosis; MRI: magnetic resonance imaging; ROIs: regions of interest; TM: temporal muscle; T2WI: T2-weighted imaging

MiR-126-5p promotes HUVECs proliferation under hypoxia via the TRPS1/ANGPT2 pathway

Given that bioinformatics analysis suggested multiple predicted binding sites for miR-126-5p on TRPS1 mRNA, as well as a potential regulatory relationship of TRPS1 with the *Angpt2* promoter, we conducted further molecular biology experiments to explore the direct regulatory effects of miR-126-5p on TRPS1 and of TRPS1 on ANGPT2. The results of the DLR assay revealed that the addition of miR-126-5p mimics to 293 T cells transfected with TRPS1 wt1, wt2 or wt3 significantly decreased the relative luciferase activity compared with the addition of mimics NC, whereas the addition of miR-126-5p mimics did not affect the relative luciferase activity of 293 T cells

transfected with TRPS1 mut1, mut2, mut3 or mut4; however, the results in 293 T cells transfected with TRPS1 wt4 were not significantly different (Fig. 6B). The RIP results revealed that, compared with the IgG antibody, the AGO2 antibody significantly enriched miR-126-5p and TRPS1 mRNAs in the immunoprecipitates (Fig. 6D). In the ChIP assay, more *Angpt2* promoter regions were detected in immunoprecipitates immunoprecipitated with TRPS1 antibodies than with IgG antibodies (Fig. 6F).

We next transfected HUVECs with miR-126-5p mimics/inhibitors and pcDNA 3.1-TRPS1/sh-TRPS1. Western blotting revealed that the expression level of TRPS1 and the ratio of pTie2/Tie2 were significantly lower in

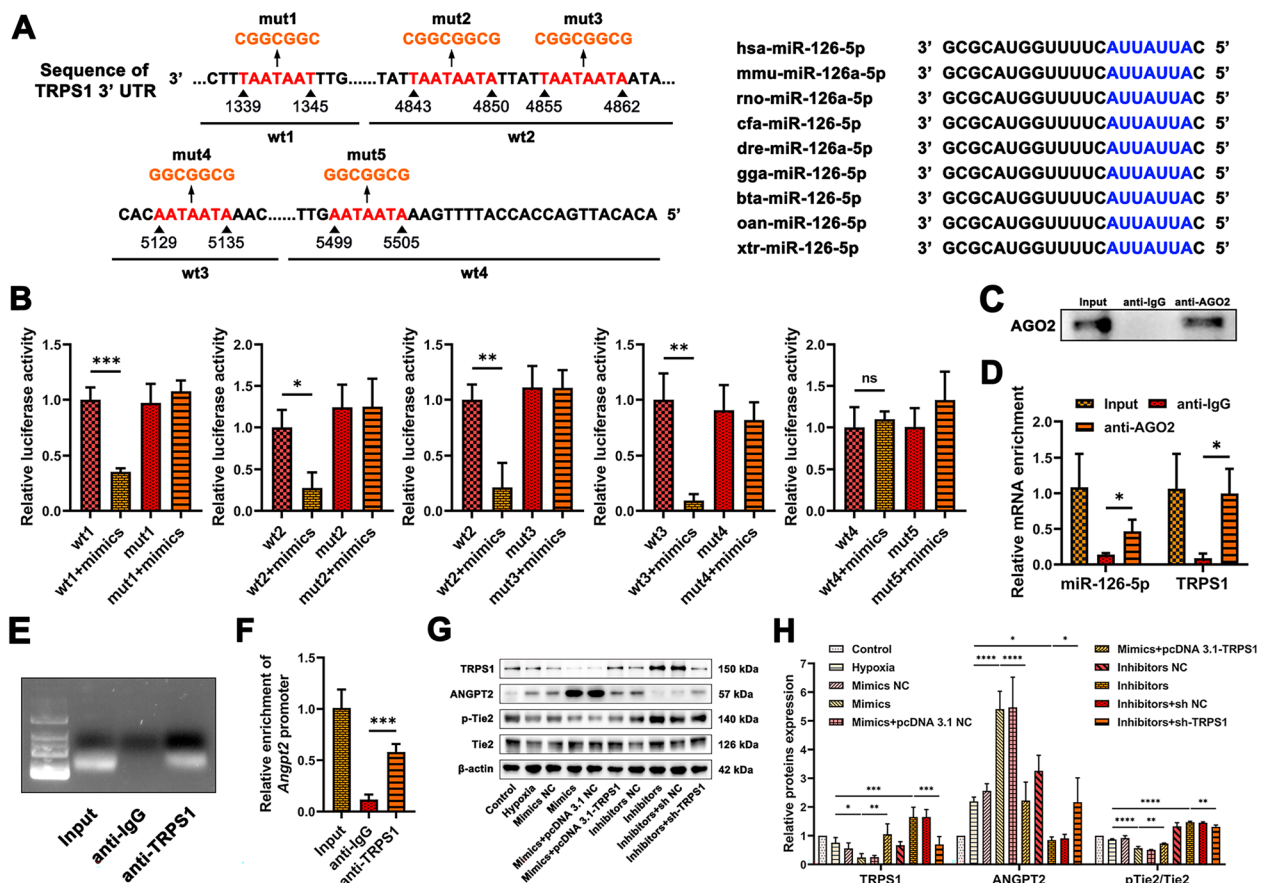
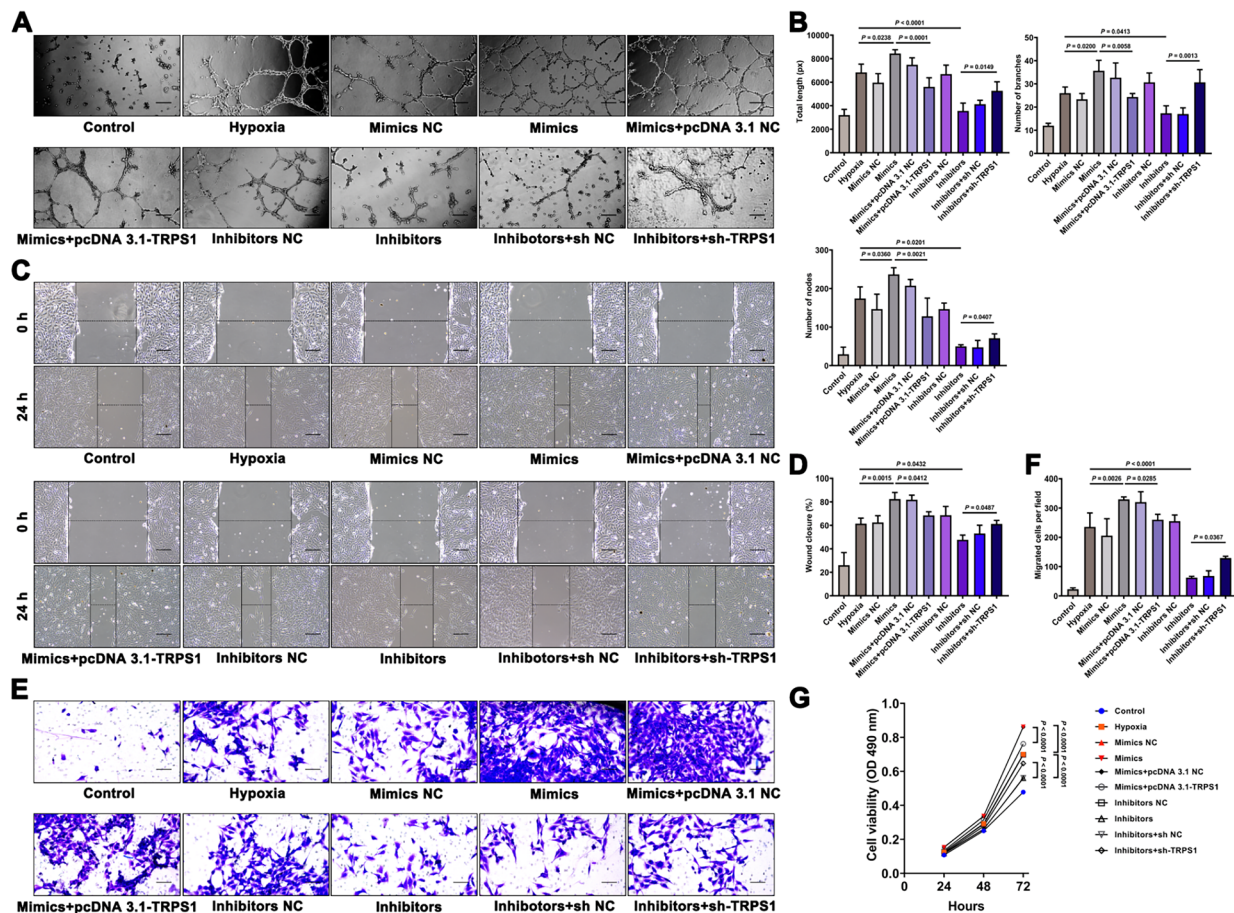


Fig. 6 Results of molecular biology experiments confirming the miR-126-5p/TRPS1/ANGPT2 pathway in vitro. **A** The predicted miR-126-5p binding sites in the 3'UTR of TRPS1 mRNA, the designed sequences of TRPS1 wt and mut, and the sequences of miR-126-5p from multiple species. **B** The results of DLR assays were determined by the relative luciferase activities (n=3, one-way ANOVA and Šidák's multiple comparisons test). **C** Western blot showing the enrichment of AGO2 in the RIP assay. **D** Column chart showing the expression levels of miR-126-5p and TRPS1 mRNA in the precipitate determined by qRT-PCR (n=3, one-way ANOVA and Šidák's multiple comparisons test). **E** Agarose gel electrophoresis image showing the molecular size of DNA after sonication (approximately 200–400 bp). **F** Column chart showing the expression levels of the *Angpt2* promoter in the precipitate determined by qRT-PCR (n=3, one-way ANOVA and Šidák's multiple comparisons test). **G** Representative western blot showing the relative expression of TRPS1, ANGPT2, pTie2, and Tie2 in the HUVECs in each group (normalized to β-actin expression). **H** Densitometric analyses of the relative expression of TRPS1, ANGPT2, and pTie2/Tie2 (n=3, one-way ANOVA and Šidák's multiple comparisons test). The error bars represent the ± SDs. * $P < 0.05$, ** $P < 0.01$, *** $P < 0.001$, **** $P < 0.0001$. ChIP: chromatin immunoprecipitation; DLR: dual luciferase reporter; RIP: RNA immunoprecipitation

the mimic group than in the hypoxia group, whereas the expression level of ANGPT2 was significantly greater in the mimic group than in the hypoxia group. The expression level of TRPS1 and the pTie2/Tie2 ratio were significantly greater in the inhibitor group than in the hypoxia group, whereas the expression level of ANGPT2 was significantly lower in the inhibitor group than in the hypoxia group. In addition, TRPS1 overexpression significantly reduced the expression level of ANGPT2 and increased the pTie2/Tie2 ratio, and the knockdown of TRPS1 significantly increased the expression level of ANGPT2 and reduced the pTie2/Tie2 ratio (Fig. 6G, H).

Next, functional experiments on the transfected HUVECs were performed. The results of the tube formation assay revealed that the total length, number of branches, and number of nodes in the mimics group were significantly greater than those in the hypoxia group ($P=0.0238$, $P=0.0200$, $P=0.0360$) and mimics+pcDNA 3.1-TRPS1 group ($P=0.0001$, $P=0.0058$, $P=0.0021$), whereas those in the inhibitors group were significantly lower than those in the hypoxia group ($P<0.0001$, $P=0.0413$, $P=0.0201$) and inhibitors+sh-TRPS1 group ($P=0.0149$, $P=0.0013$, $P=0.0407$) (Fig. 7A, B). The results of the scratch wound assay revealed that the wound closure percentage in the



mimics group was significantly greater than that in the hypoxia group ($P=0.0015$) and mimics+pcDNA 3.1-TRPS1 group ($P=0.0412$), whereas that in the inhibitors group was significantly lower than that in the hypoxia group ($P=0.0432$) and the inhibitors+sh-TRPS1 group ($P=0.0487$) (Fig. 7C, D). The results of the Transwell migration assay revealed that the number of migrated cells in the mimics group was significantly greater than that in the hypoxia group ($P=0.0026$) and the mimics+pcDNA 3.1-TRPS1 group ($P=0.0285$), whereas that in the inhibitors group was significantly lower than that in the hypoxia group ($P<0.0001$) and the inhibitors+sh-TRPS1 group ($P=0.0367$) (Fig. 7E, F). MTT assays revealed that the cell viability at 72 h of the

mimics group was significantly greater than that of the hypoxia group ($P<0.0001$) and the mimics+pcDNA 3.1-TRPS1 group ($P<0.0001$), whereas that of the inhibitors group was significantly lower than that of the hypoxia group ($P<0.0001$) and the inhibitors+sh-TRPS1 group ($P<0.0001$) (Fig. 7G).

TEMs promote angiogenesis in CIBT of rats via the miR-126-5p/TRPS1/ANGPT2 pathway

We established a 2VO+EMS model in SD rats, injected a miR-126-5p agomir/antagomir into their TM tissue and LV-ANGPT2/LV-sh-ANGPT2 into their lateral ventricles. The results of the MRI-ASL sequence revealed that the rats in the agomir group presented significantly

greater perfusion ratios than did the rats in the control group ($P=0.0033$) and the agomir+LV-sh-ANGPT2 group ($P<0.0001$). The rats in the antagomir group presented significantly lower perfusion ratios than the rats in the control group ($P=0.0491$) and the antagomir+LV-ANGPT2 group ($P=0.0389$) did (Fig. 8A, B). The NORT results revealed that the rats in the agomir group recognized the novel object significantly more often than did the rats in the control group ($P=0.0113$)

and the agomir+LV-sh-ANGPT2 group ($P=0.0005$). Moreover, the proportion of rats in the antagomir group that recognized the novel object was significantly lower than that in the control group ($P=0.0012$) and antagomir+LV-ANGPT2 group ($P=0.0187$) (Fig. 8C, D). In the MWM tests, compared with those in the control and agomir+LV-sh-ANGPT2 groups, the rats in the agomir groups had significantly shorter escape latencies on day 5 ($P<0.0001$, $P=0.0255$), longer durations in

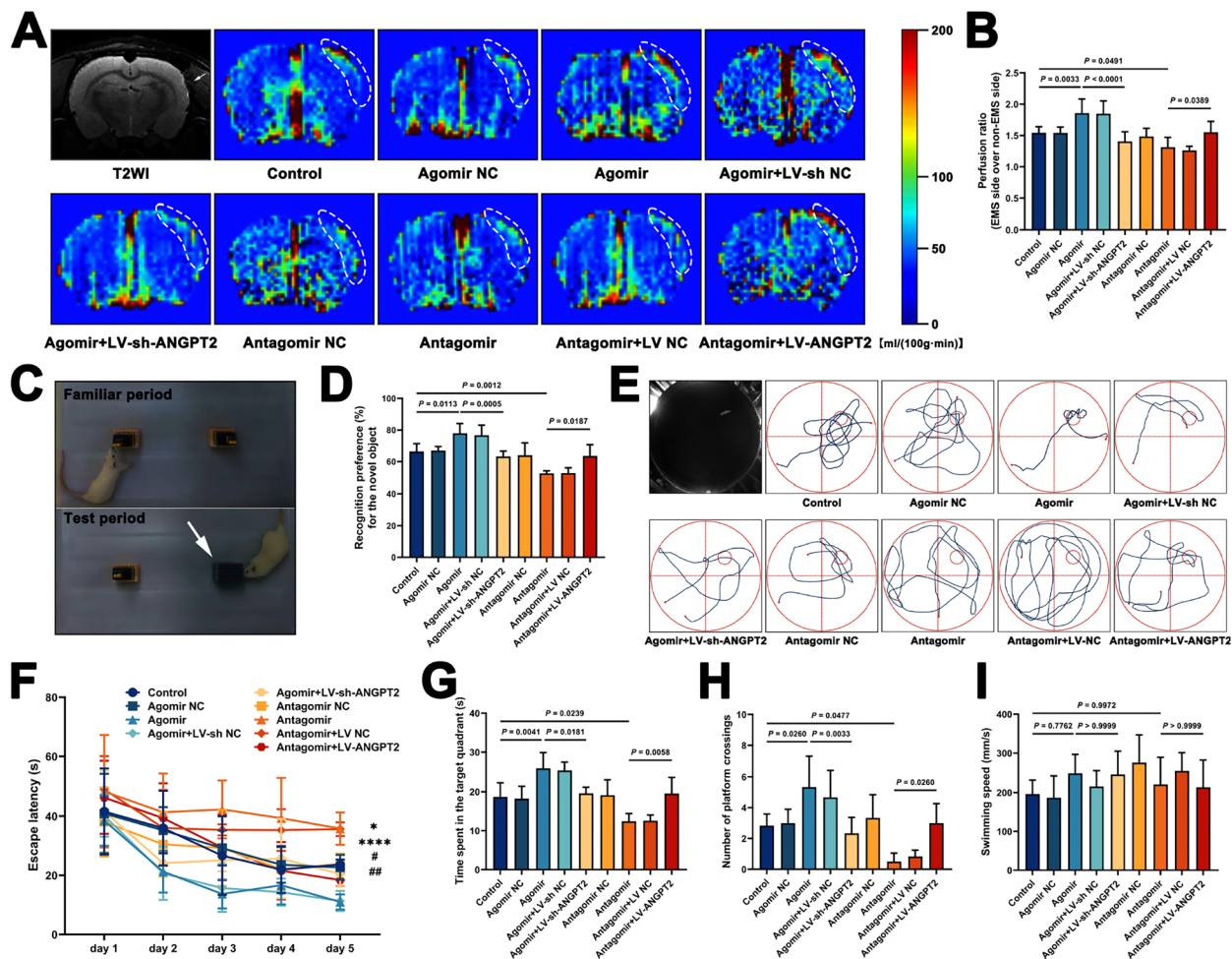


Fig. 8 Results of the MIR-ASL scanning and the behavioural test for 2VO+EMS rats. **A** Representative MRI-T2WI film showing the EMS surgical site (white arrow) and MIR-ASL films showing differences in CBP between the various groups (white dashed lines indicate ROIs under the EMS surgical site). **B** Column chart showing the perfusion ratios (EMS sides over non-EMS sides) of each group ($n=6$, one-way ANOVA and Šidák's multiple comparisons test). **C** Procedures of the NORT (the white arrow indicates the novel object). **D** The NORT results were quantified by the percentage of time the rats took to recognize the novel object ($n=6$, one-way ANOVA and Tukey's multiple comparisons test). **E** Representative image showing the procedure of the MWM test and swimming paths obtained from each group in the MWM test. **F** Line chart showing the average escape latencies in each group ($n=6$, two-way ANOVA and Tukey's multiple comparisons test; **** $P<0.0001$, agomir group versus control group; * $P=0.0255$, agomir group versus agomir+LV-sh-ANGPT2 group; # $P=0.0253$, antagomir group versus control group; ## $P=0.0035$, antagomir group versus antagomir+LV-ANGPT2 group). Column charts showing **G** the time spent in the target quadrant, **H** the number of platform crossings and **I** swimming speed among the groups ($n=6$, one-way ANOVA and Tukey's multiple comparisons test). The error bars represent the \pm SDs. ASL: arterial spin labelling; CBP: cerebral blood perfusion; EMS: encephalomyosynangiosis; MRI: magnetic resonance imaging; MWM: Morris water maze; NORT: novel object recognition test; ROIs: regions of interest; T2WI: T2-weighted imaging; 2VO: 2-vessel occlusion

the target quadrant ($P=0.0041$, $P=0.0181$) and greater numbers of platform crossings ($P=0.0260$, $P=0.0033$) on the test day. In contrast, the rats in the antagomir group had a significantly longer escape latency on day 5, shorter time spent in the target quadrant and fewer platform crossings on the test day than did those in the control group ($P=0.0253$, $P=0.0239$, $P=0.0477$) and the antagomir + LV-ANGPT2 group ($P=0.0035$, $P=0.0058$, $P=0.0260$). However, there was no significant difference in swimming speed among the groups (Fig. 8E–I).

We next harvested brain tissues from the rats for pathological experiments and the detection of downstream molecules. The results of transmission electron microscopy revealed that the average number of vacuoles per 10 μm and the proportion of abnormal TJs were significantly lower in the brain tissue around the EMS site in the rats in the agomir group than in those in the control group and the agomir + LV-sh-ANGPT2 group ($P=0.0445$, $P=0.0012$, agomir group versus control group; $P=0.0027$, $P=0.0018$, agomir group versus agomir + LV-sh-ANGPT2 group). The average number of vacuoles per 10 μm and the proportion of abnormal TJs were significantly greater in the brain tissue around the EMS site of the rats in the antagomir group than in those in the control group and antagomir + LV-ANGPT2 group ($P=0.0033$, $P=0.0169$, antagomir group versus control group; $P=0.0060$, $P=0.0019$, antagomir group versus antagomir + LV-ANGPT2 group) (Fig. 9A, B). Scanning electron microscopy revealed that the morphology of pericytes in the brain tissue around the EMS site in the rats in the agomir group was fuller compared with that in the control group and agomir + LV-sh-ANGPT2 group, and the surrounding finger-like extensions were longer and more abundant. The morphology of pericytes in the brain tissue around the EMS site in the antagomir group was atrophied compared with that in the control group and agomir + LV-ANGPT2 group, and the peripheral finger-like extensions were lacking (Fig. 9C).

The immunofluorescence results revealed that the counts of ANGPT2⁺, VEGFA⁺, and IGF1⁺ cells, TEMs (Tie2⁺/CD11b⁺), and ECs (CD31⁺) in the agomir group were significantly greater than those in the control group and agomir + LV-sh-ANGPT2 group. The counts of ANGPT2⁺, VEGFA⁺, and IGF1⁺ cells, TEMs (Tie2⁺/CD11b⁺), and ECs (CD31⁺) in the antagomir group were significantly lower than those in the control group and antagomir + LV-ANGPT2 group (Figs. 10A–C, 11, Figure S5). The results of western blotting revealed that the expression level of TRPS1 in the brain tissues around the EMS site in the rats in the agomir group was significantly lower but the expression levels of ANGPT2, Tie2, CD11b, VEGFA, IGF1, and CD31 were significantly greater than those in the control group. The changes in the expression

levels of ANGPT2, Tie2, CD11b, VEGFA, IGF1, and CD31 were reversed by the knockdown of ANGPT2, whereas the expression level of TRPS1 was not affected. The expression level of TRPS1 in the brain tissues of the rats in the antagomir group was significantly greater but the expression levels of ANGPT2, Tie2, CD11b, VEGFA, IGF1, and CD31 were significantly lower than those in the control group. The changes in the expression levels of ANGPT2, Tie2, CD11b, VEGFA, IGF1, and CD31 were reversed by the overexpression of ANGPT2, whereas the expression level of TRPS1 was not affected (Fig. 10D, E).

Discussion

Tie is a type of ANGPT receptor that includes Tie1 and Tie2. Tie1 is expressed in ECs and a few haematopoietic stem cells. It does not bind directly to ANGPT but regulates Tie2 activity through heterodimerization. Tie2 is a specific receptor of ANGPT. It is expressed mainly in ECs and regulates vascular stability and remodelling through the ANGPT-Tie2 axis [30, 31]. ANGPT1 and ANGPT2, members of the ANGPT family, have an antagonistic competitive relationship: they competitively bind to Tie2 on the surface of ECs [32]. ANGPT1 binding to Tie2 promotes the phosphorylation of Tie2, thereby promoting vascular maturation and stability, whereas ANGPT2 binding to Tie2 inhibits its phosphorylation, which induces vascular destabilization and promotes angiogenesis [31, 33, 34].

The recent discovery of TEMs has expanded research on Tie2. This type of tumour-associated monocyte/macrophage was first discovered by De Palma's team in breast cancer research [6] and has recently been shown to facilitate tumour growth by promoting tumour angiogenesis [4, 5, 7–9]. In addition, the proangiogenic effect of TEMs was confirmed in nontumor ischaemic tissues (such as ischaemic tissues, such as ischaemic limbs [10, 11] and brain tissue surrounding acute cerebral infarction [12]). Given that the degree of cerebral angiogenesis after revascularization surgery in CIBD patients is crucial for the prevention of stroke, whether TEMs can play the same role in CIBT has become a research direction. In this study, we revealed that the proportion of TEMs in the IJV blood from CIBD patients was significantly increased like some patients with malignant tumours [35–37]. Moreover, the proportion of TEMs in the IJV blood from Matsushima Grade-A patients (better angiogenesis) was significantly greater than that from Matsushima Grade-C patients (poorer angiogenesis), indicating that more TEMs infiltrating the brain of CIBD patients may lead to better angiogenesis and revascularization effects. Given the above results and based on Sheng's [12] recent findings that TEMs can promote angiogenesis in the brain tissue surrounding acute cerebral infarction, we

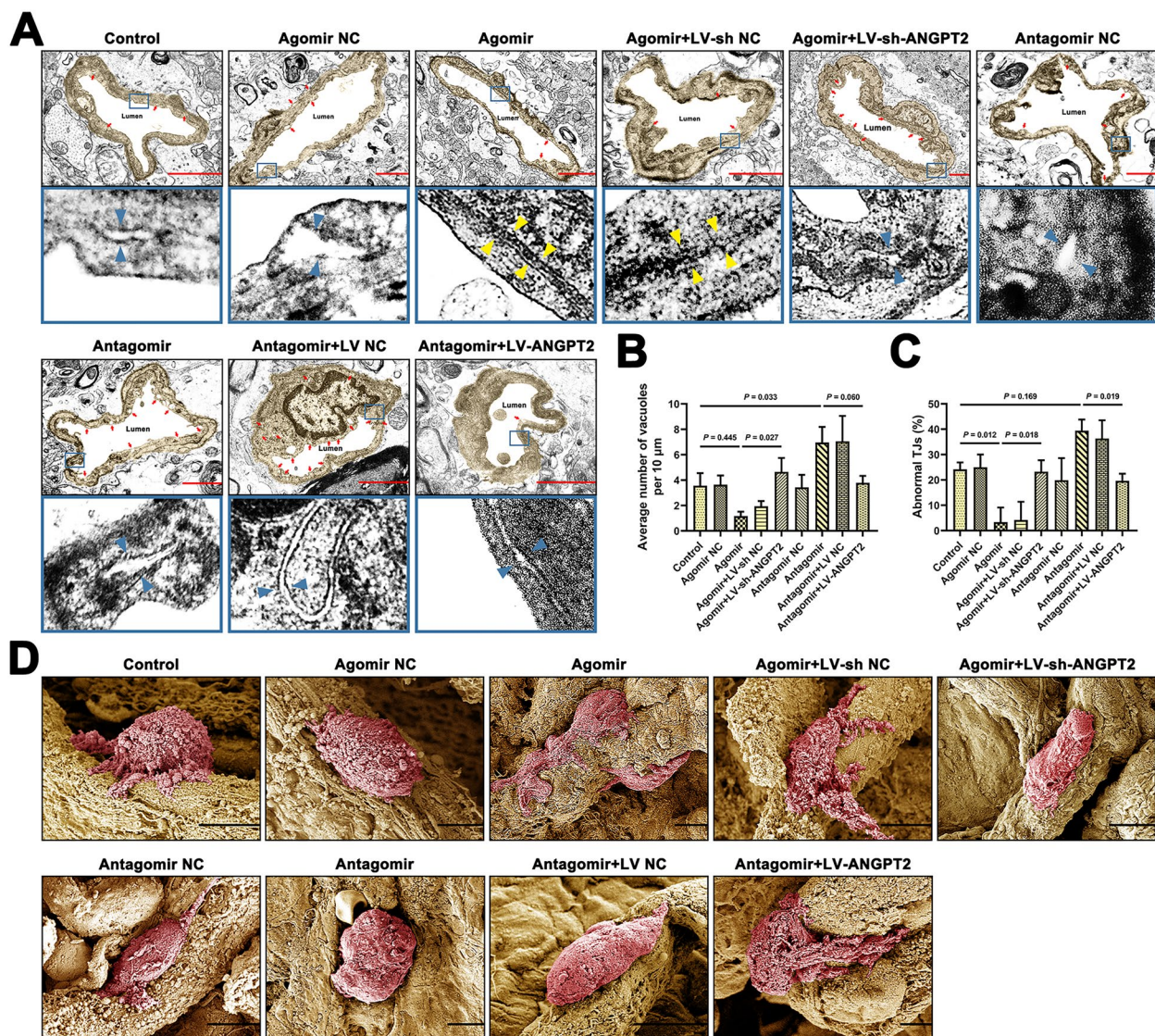


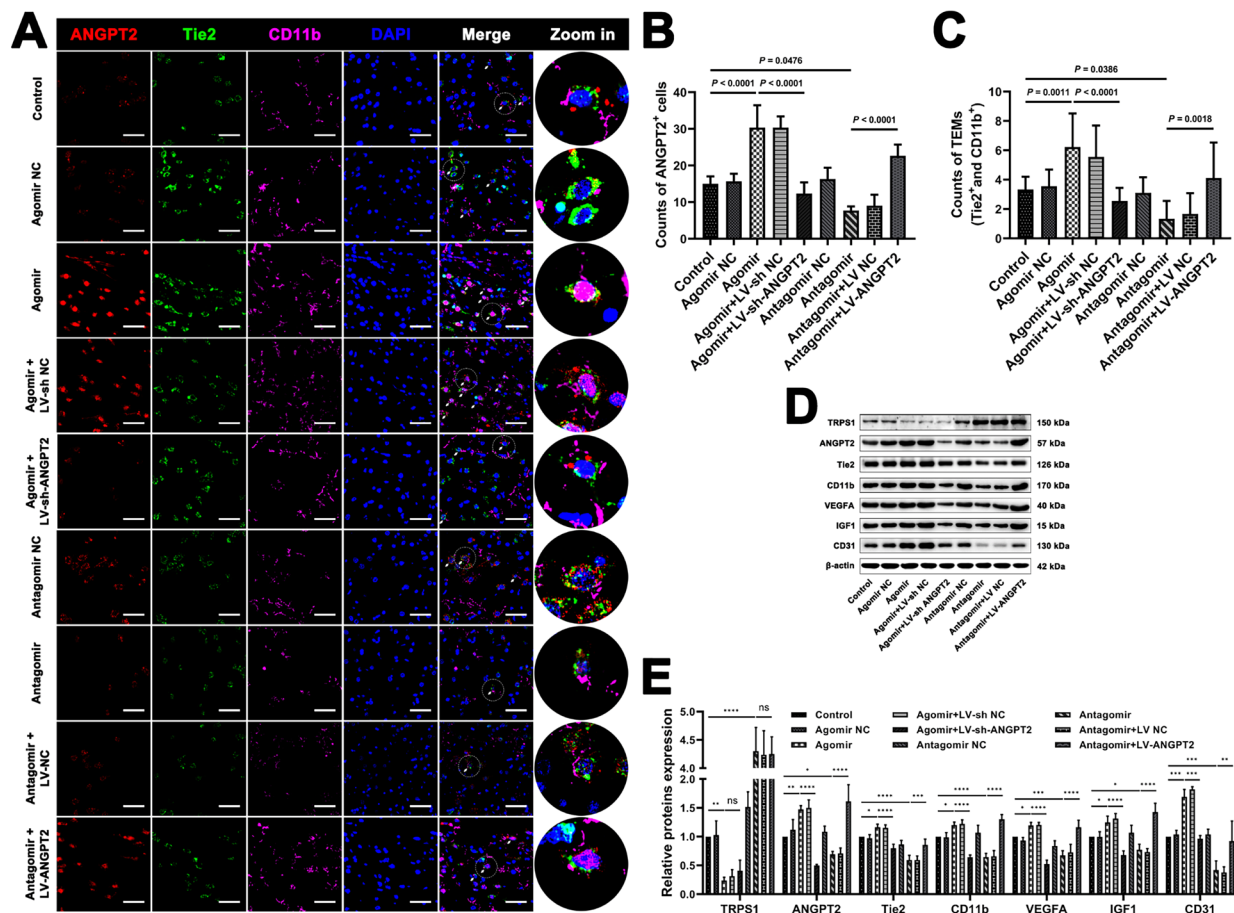
Fig. 9 Electron microscopic results of CIBT for 2VO + EMS rats. **A** Representative transmission electron microscopic images showing the morphology of ECs in each group (the red arrows indicate vacuoles; the yellow arrows indicate normal TJs; the blue arrows indicate abnormal TJs). Bar = 2 μm . **B** Average number of vacuoles per 10 μm and **C** the proportion of abnormal TJs indicating the EC function of each group ($n = 3$, one-way ANOVA and Šidák's multiple comparisons test). **D** Representative scanning electron microscopic images showing the morphology of pericytes in each group. Bar = 5 μm . The error bars represent the \pm SDs. CIBT: chronically ischaemic brain tissue; ECs: endothelial cells; EMS: encephalomyosynangiosis; TJs: tight junctions; 2VO: 2-vessel occlusion

focused on whether TEMs exhibit proangiogenic effects in CIBT.

To confirm the proliferative effect of TEMs on ECs in vitro, we directly and indirectly cocultured TEMs with HUVECs under hypoxic conditions. The results indicated that TEMs promoted HUVEC proliferation and inhibited HUVEC apoptosis via the two coculture methods. Additionally, the lack of a significant difference in the proliferation and apoptosis levels of HUVECs between the two coculture methods suggested that the proangiogenic

effect of TEMs may be achieved through a paracrine mechanism, which was reported in previous studies [13, 14]. Moreover, we found that the promoting effect of TEMs on HUVECs is concentration-dependent. This promoting effect was also verified in vivo via nude mouse experiments.

Considering that TEMs are immune cells and originate from different species (humans), the use of nude mice with innate immune deficiency for in vivo experiments can effectively prevent immune rejection. Moreover,



Patel's team explored the angiogenic effect of TEMs in vivo by injecting them into the ischaemic lower limb muscles of nude mice [10], which indicated the feasibility of directly injecting TEMs into ischaemic lesions of nude mice to verify their ability to promote angiogenesis. Therefore, we constructed a microenvironment for cerebral angiogenesis in CIBT by performing EMS surgery on BALB/c nude mice after ICAO procedure and directly injected TEMs into the lateral ventricles of nude mice to facilitate their recruitment into ischaemic brain tissue. Consistent with our in vitro experiments and Patel's research [10], the results showed that TEMs effectively promoted EC proliferation and angiogenesis in CIBT, and significantly improved CBP in nude mice with ICAO.

In addition, TEMs promoted angiogenesis in CIBT in a concentration-dependent manner consistent with coculture experiments. These findings suggest that regulating the recruitment of TEMs to increase their infiltration in CIBT may become a new therapeutic strategy for promoting angiogenesis and revascularization in CIBT.

The role of the ANGPT2/Tie2 axis in regulating EC proliferation and angiogenesis has been validated in various models [33, 38–40]. Owing to the presence of Tie2 receptors on the surface of TEMs, the ANGPT2/Tie2 axis also plays a crucial role in regulating the biological function of TEMs. Moreover, Murdoch's team demonstrated in vitro that ANGPT2 is a chemotactic factor of TEMs [8]. On the basis of the above information, we

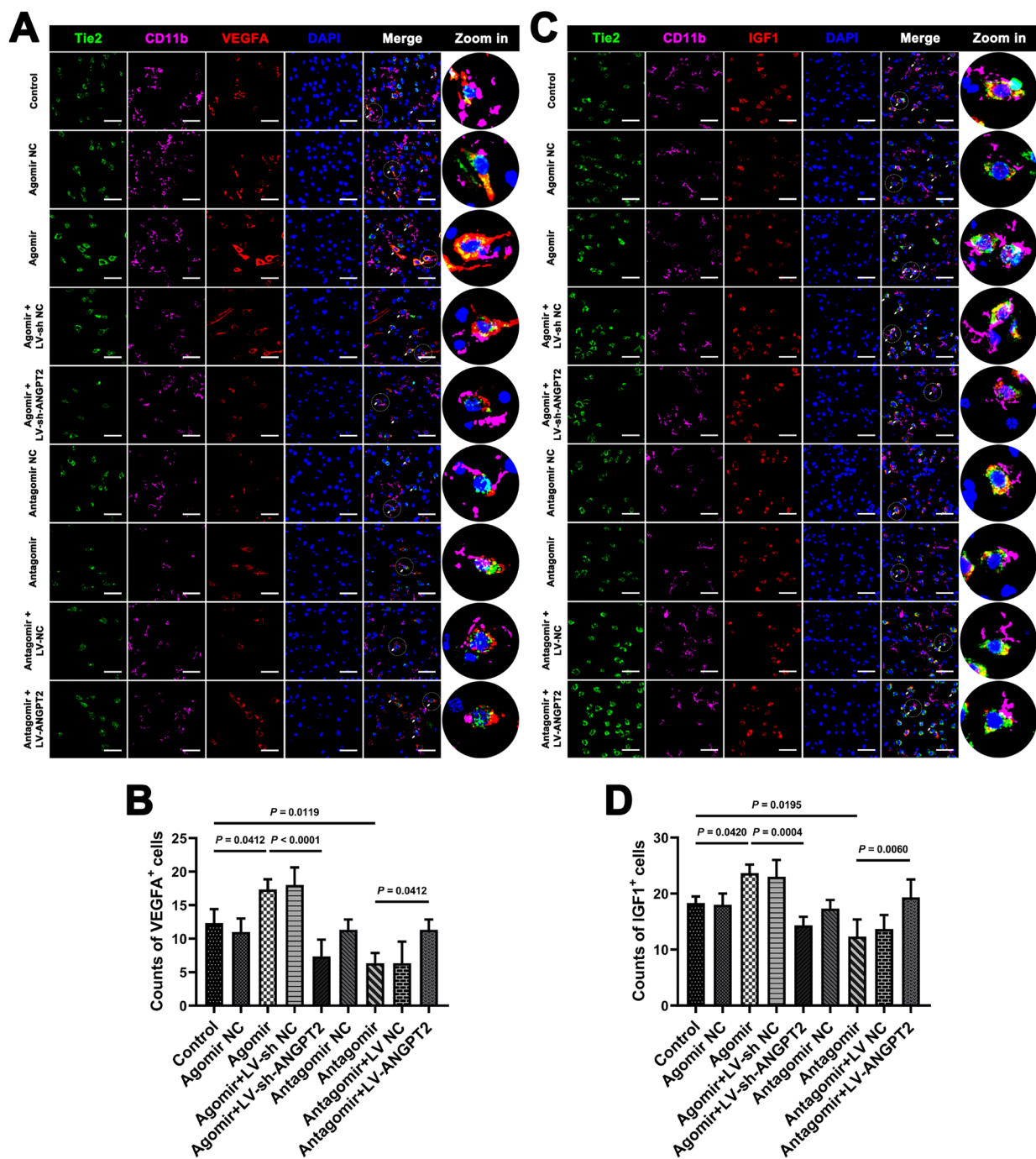


Fig. 11 Immunofluorescence results showing the expression of pro-angiogenesis factors in the CIBT of 2VO + EMS rats. **A** Representative triple immunofluorescence staining images showing Tie2⁺, CD11b⁺, and VEGFA⁺ cells and in the CIBT in each group (white arrows indicate TEMs). Bar = 50 μ m. **B** Counts of VEGFA⁺ cells in each group (n = 3, one-way ANOVA and Šidák's multiple comparisons test). **C** Representative triple immunofluorescence staining images showing Tie2⁺, CD11b⁺, and IGF1⁺ cells in the CIBT in each group (white arrows indicate TEMs). Bar = 50 μ m. **D** Counts of IGF1⁺ cells in each group (n = 3, one-way ANOVA and Šidák's multiple comparisons test). CIBT: chronically ischaemic brain tissue; EMS: encephalomyosynangiosis; TEMs: Tie2-expressing monocytes/macrophages; 2VO: 2-vessel occlusion

focused on the mechanisms that regulate the expression of ANGPT2.

MiR-126-5p is a miRNA specific to ECs, and its ability to promote EC proliferation has been widely reported [16–19]. Although miR-126-5p is expressed mainly in ECs, a few studies have shown that it can also be expressed in monocytes and macrophages [41, 42]. Therefore, the following question arises: can TEMs promote EC proliferation through the release of miR-126-5p? The DIANA-miTED database revealed that the expression of miR-126-5p in CD14⁺ monocytes was only 1/23 that in capillary ECs (Figure S6A) [43]. Moreover, our study revealed that coculture of HUVECs with TEMs did not increase the expression of miR-126-5p in HUVECs and that intraventricular injection of TEMs did not increase the expression of miR-126-5p in the CIBT of nude mice (Figure S6B–C). These results indicated that (1) TEM is unlikely to promote angiogenesis by expressing and releasing miR-126-5p itself, and (2) even if TEMs can release miR-126-5p, the amount is likely negligible compared with the level of miR-126-5p in ECs. Therefore, studies on the role of miR-126-5p in promoting angiogenesis should focus on its expression in ECs rather than in TEMs. However, the downstream regulatory mechanism of miR-126-5p is still unclear.

TRPS1, an oncogene, is widely expressed in various malignant tumours and has been confirmed to participate in the regulation of EC proliferation in tumour tissues [22–24]. MiRNAs play important roles in the

regulation of TRPS1. For example, miR-222-3p targets TRPS1, promoting the invasion and metastasis of renal cell cancer [44], and miR-373 downregulates the expression of TRPS1, promoting the epithelial–mesenchymal transition of breast cancer [45]. Additionally, both the miRDB and TargetScan databases predicted that many miRNAs may be upstream regulators of TRPS1, among which miR-126-5p was highly correlated with angiogenesis [25, 26]. Bioinformatics analysis suggested that (1) TRPS1 is likely a downstream gene of miR-126-5p, and (2) TRPS1 is a special member of the GATA transcription factor family and may act on the GRE in the *Angpt2* promoter sequence to regulate the expression of ANGPT2 (Figure S1).

On the basis of the above information, we first performed molecular experiments such as DLR, RIP and ChIP assays to determine the direct regulatory relationship between miR-126-5p/TRPS1 and TRPS1/ANGPT2 at the molecular level. The results revealed that (1) miR-126-5p can directly bind to TRPS1 mRNA and that (2) TRPS1 can directly bind to the GRE in the promoter of *Angpt2*. To clarify the regulatory relationship of the miR-126-5p/TRPS1/ANGPT2 pathway and its impact on EC proliferation in vitro, we cotransfected HUVECs with miR-126-5p mimics/inhibitors and TRPS1 overexpression/knockdown plasmids and found that miR-126-5p can downregulate TRPS1, upregulate ANGPT2, reduce the degree of phosphorylation of Tie2 receptors and promote HUVECs proliferation. However, these effects

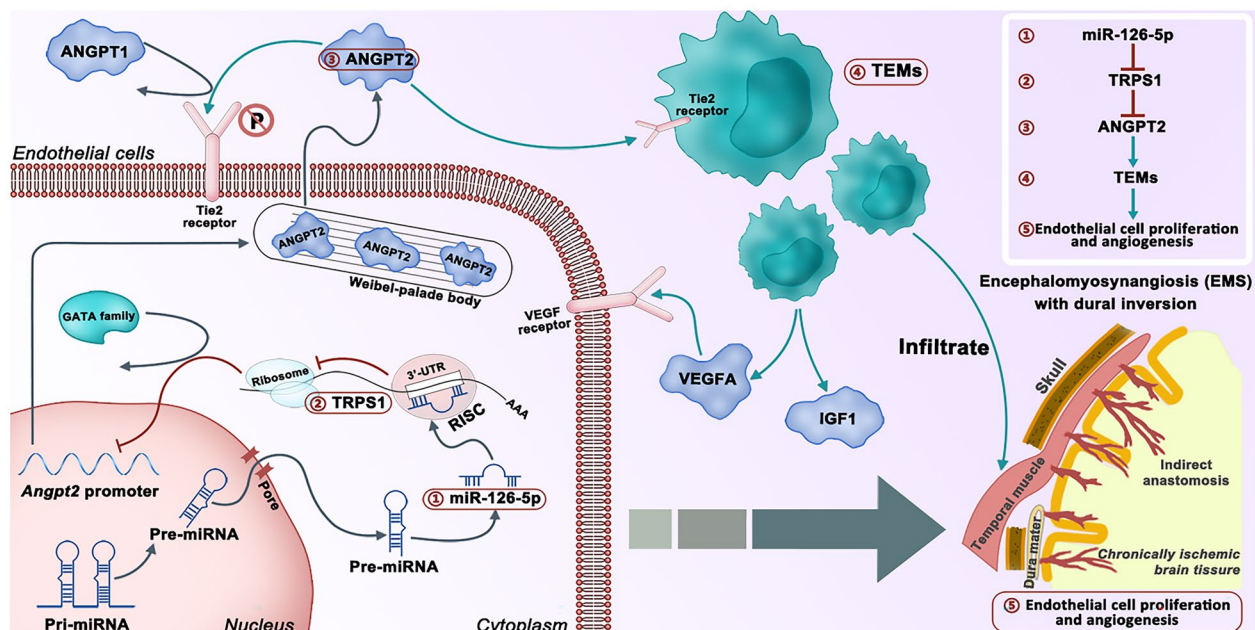


Fig. 12 Schematic diagram showing that Tie2-expressing monocytes/macrophages are recruited to chronically ischaemic brain tissue via the miR-126-5p/TRPS1/ANGPT2 pathway to promote the proliferation of endothelial cell and angiogenesis

were reversed by overexpression of TRPS1. These results indicated that the transcription of ANGPT2 was inhibited by TRPS1, the translation of TRPS1 was inhibited by miR-126-5p, and the miR-126-5p/TRPS1/ANGPT2 pathway further acted on Tie2 receptors on the surface of HUVECs and ultimately altered their activity. These findings preliminarily confirm that the biological functions and phenomena related to the Tie2 receptor are regulated by the miR-126-5p/TRPS1/ANGPT2 pathway.

In animal experiments, we used 2VO+EMS in SD rats to construct a microenvironment for angiogenesis in CIBT of rats and injected the miR-126-5p agomir/antagomir into the TM tissue and the ANGPT2 overexpression/knockdown lentivirus into the lateral ventricle to explore the regulatory effect of the miR-126-5p/TRPS1/ANGPT2 pathway on TEMs recruitment in CIBT and the ability of infiltrating TEMs to promote angiogenesis. Consistent with previous studies [12, 46, 47], our study revealed that high expression of ANGPT2 in CIBT leads to increased infiltration of TEMs as well as increased angiogenesis and revascularization and that ANGPT2 is regulated by miR-126-5p/TRPS1. The validation that the miR-126-5p/TRPS1/ANGPT2 pathway regulates the recruitment of TEMs provides a novel interpretation of the mechanism by which miR-126-5p promotes EC proliferation. Moreover, we found that the expression of VEGFA and IGF1 increased with the infiltration of TEMs, further demonstrating that TEMs promote EC proliferation and angiogenesis through a paracrine mechanism.

In addition, as inflammatory cells, TEMs are involved in the regulation of inflammation in the tumour microenvironment via the PI3K/Akt/mTOR and JAK/STAT pathways and infiltrate acute lung injury and rheumatoid arthritis [48, 49]. After being recruited by ANGPT2, infiltrating TEMs secrete inflammatory-related factors such as IL-10 and polarize into M2 macrophages, which can suppress T-cell activation, promote regulatory T-cell expansion, and release proangiogenic factors [50–52]. These effects create a suitable microenvironment for EC proliferation. Inflammation also occurs in ischaemic tissues and plays a dual role in regulating angiogenesis [53, 54]. Some inflammatory factors, such as TNF- α , IL-1 and IL-6, can promote EC proliferation [54–56]; however, the large amount of reactive oxygen species (ROS) produced by excessive inflammation activation can also damage ECs and is not conducive to angiogenesis [57]. TEMs may also promote EC proliferation and angiogenesis indirectly by regulating inflammation.

This study has several limitations. First, the specific mechanism by which TEMs promote EC proliferation after recruitment to CIBT is still unclear. Second, 2VO is the most commonly used animal model for chronic cerebral ischaemia modelling. However, the application of

2VO in BALB/c nude mice resulted in an increased mortality rate, so we used ICAO to establish a chronic cerebral ischaemia model in nude mice. The results showed that implementing ICAO+EMS in nude mice can also generate a microenvironment conducive to angiogenesis in CIBT. Third, the extensive exercise in the MWM test may have interfered with the results of the subsequent experiments. Fourth, the 2VO+EMS rat modelling procedures are relatively complicated and time-consuming, which prevents the use of a larger sample size in *in vivo* experiments to support our conclusions.

Conclusion

TEMs can promote EC proliferation and angiogenesis through a paracrine mechanism in CIBT. The recruitment process of TEMs to CIBT is regulated by the miR-126-5p/TRPS1/ANGPT2 pathway. Improving the infiltration of TEMs in CIBT may be a new therapeutic strategy for CIBT treatment (Fig. 12).

Abbreviations

ANGPT2	Angiopoietin-2
ASL	Arterial spin labelling
BCA	Bicinchoninic acid
BSA	Bovine serum albumin
CBF	Cerebral blood flow
CBP	Cerebral blood perfusion
ChIP	Chromatin immunoprecipitation
CIBT	Chronically ischaemic brain tissue
CICD	Chronically ischaemic cerebrovascular disease
CTP	Computed tomography perfusion
DLR	Dual luciferase reporter
DM	Dura mater
DMEM	Dulbecco's modified Eagle's medium
DSA	Digital subtraction angiography
ECs	Endothelial cells
ECL	Enhanced chemiluminescence
EDU	Ethynyl deoxyuridine
ELASA	Enzyme-linked immunosorbent assay
EMS	Encephalomyosynangiosis
FBS	Foetal bovine serum
GRE	GATA regulatory element
HUVECs	Human umbilical vein endothelial cells
ICA	Internal carotid artery
ICAO	Internal carotid artery occlusion
IJV	Internal jugular vein
LV	Lentivirus
MACS	Magnetic-activated cell sorting
MCA	Middle cerebral artery
MRI	Magnetic resonance imaging
MTT	Methylthiazolyldiphenyl-tetrazolium bromide
MWM	Morris water maze
NORT	Novel object recognition test
NS	Normal saline
OD	Optical density
PBMCs	Peripheral blood mononuclear cells
PBS	Phosphate buffer solution
PFA	Paraformaldehyde
PMSF	Phenylmethanesulfonyl fluoride
PVDF	Polyvinylidene fluoride
RIP	RNA immunoprecipitation
RIPA	Radioimmunoprecipitation assay
ROIs	Regions of interest
RPMI	Roswell Park Memorial Institute

SPF	Specific pathogen-free
TBS	Tris-buffered saline
TBST	Tris-buffered saline containing 0.2% Tween-20
TEMs	Tie2-expressing monocytes/macrophages
TM	Temporal muscle
TNMs	Tie2-negative monocytes/macrophages
TRPS1	Transcriptional repressor GATA binding 1
TJs	Tight junctions
T2WI	T2-weighted imaging
2VO	2-Vessel occlusion

Supplementary Information

The online version contains supplementary material available at <https://doi.org/10.1186/s13578-025-01401-1>.

Supplementary material 1.

Acknowledgements

The authors wish to thank Qingyang Liu for the excellent technical support.

Author contributions

CT: Writing—original draft, formal analysis, methodology, investigation; CL: Writing—original draft, formal analysis, methodology, investigation; YY: Writing—original draft, formal analysis, methodology, investigation; BZ: Writing—review and editing, data curation, investigation; JS: Writing—review and editing, visualization, investigation; NM: Writing—review and editing, visualisation, investigation; TS: Writing—review and editing, Validation; LH: Writing—review and editing, validation; CY: Writing—review and editing; HW: Writing—review and editing, conceptualization, supervision; CC: Writing—review and editing, conceptualization, supervision, funding acquisition. All authors read and approved the final manuscript.

Funding

This research was supported by the Key Technologies Research and Development Program of Guangzhou Municipality under Grant No. 2023B03J0191, the Basic and Applied Basic Research Foundation of Guangdong Province under Grant No. 2025A1515012390, the Research Project of Yuedong Hospital, the Third Affiliated Hospital of Sun Yat-sen University, under Grant No. YDC2022001, and the Basic Scientific Research Funds of Sun Yat-sen University (Young Teacher Training Project) under Grant No. b202408011053050001.

Availability of data and materials

The datasets used and/or analysed during the current study are available from the corresponding author on reasonable request.

Declarations

Ethics approval and consent to participate

The human-related research in this study followed the Declaration of Helsinki (2000) and was approved by the Ethics Committee of the Third Affiliated Hospital of Sun Yat-sen University (No. RG2023-225-02). Written informed consent was obtained from all the participants. The animal experiments were performed in compliance with the ARRIVE guidelines and approved by the Animal Ethics Committee of Guangzhou Huateng Biopharmaceutical Technology Co., Ltd. (IACUC No. C202301-2).

Consent for publication

Not applicable.

Competing interests

The authors declare no conflicts of interest.

Author details

¹Department of Neurosurgery, Third Affiliated Hospital of Sun Yat-Sen University, No. 600 Tianhe Road, Tianhe District, Guangzhou, , Guangdong, People's Republic of China. ²Department of Radiology, Third Affiliated Hospital of Sun Yat-Sen University, No. 600 Tianhe Road, Guangzhou, Guangdong, People's Republic of China.

Received: 18 November 2024 Accepted: 27 April 2025

Published online: 21 May 2025

References

- Global, regional, and national burden of stroke and its risk factors, 1990–2019: a systematic analysis for the Global Burden of Disease Study 2019. *Lancet Neurol.* 2021;20(10):795–820.
- World health statistics 2024: monitoring health for the SDGs, sustainable development goals: World Health Organization; 2024. <https://iris.who.int/handle/10665/376869>.
- Powers WJ, Rabinstein AA, Ackerson T, Adeoye OM, Bambakidis NC, Becker K, et al. 2018 Guidelines for the early management of patients with acute ischemic stroke: a guideline for Healthcare Professionals From the American Heart Association/American Stroke Association. *Stroke.* 2018;49(3):e46–110.
- Matsubara T, Kanto T, Kuroda S, Yoshio S, Higashitani K, Kakita N, et al. Tie2-expressing monocytes as a diagnostic marker for hepatocellular carcinoma correlates with angiogenesis. *Hepatology.* 2013;57(4):1416–25.
- Coffelt SB, Tal AO, Scholz A, De Palma M, Patel S, Urbich C, et al. Angiopoietin-2 regulates gene expression in Tie2-expressing monocytes and augments their inherent proangiogenic functions. *Cancer Res.* 2010;70(13):5270–80.
- De Palma M, Venneri MA, Galli R, Sergi L, Politi LS, Sampaoli M, et al. Tie2 identifies a hematopoietic lineage of proangiogenic monocytes required for tumor vessel formation and a mesenchymal population of pericyte progenitors. *Cancer Cell.* 2005;8(3):211–26.
- Venneri MA, De Palma M, Ponzoni M, Pucci F, Scielzo C, Zonari E, et al. Identification of proangiogenic Tie2-expressing monocytes (TEMs) in human peripheral blood and cancer. *Blood.* 2007;109(12):5276–85.
- Murdoch C, Tazzyman S, Webster S, Lewis CE. Expression of Tie-2 by human monocytes and their responses to angiopoietin-2. *J Immunol.* 2007;178(11):7405–11.
- Lewis CE, De Palma M, Naldini L. Tie2-expressing monocytes and tumor angiogenesis: regulation by hypoxia and angiopoietin-2. *Cancer Res.* 2007;67(18):8429–32.
- Patel AS, Smith A, Nucera S, Bizziato D, Saha P, Attia RQ, et al. Tie2-expressing monocytes/macrophages regulate revascularization of the ischemic limb. *EMBO Mol Med.* 2013;5(6):858–69.
- Dopheide JF, Geissler P, Rubrecht J, Trumm P, Zeller GC, Bock K, et al. Inflammation is associated with a reduced number of pro-angiogenic Tie-2 monocytes and endothelial progenitor cells in patients with critical limb ischemia. *Angiogenesis.* 2016;19(1):67–78.
- Sheng Y, Duan X, Liu Y, Li F, Ma S, Shang X, et al. Tie2-expressing monocytes/macrophages promote cerebral revascularization in peri-infarct lesions upon ischemic insult. *Signal Transduct Target Ther.* 2021;6(1):295.
- Yin X, Zhang B, Chen L, Xia W, Liu G, Zhu X, et al. Essential contribution of macrophage Tie2 signalling in a murine model of laser-induced choroidal neovascularization. *Sci Rep.* 2020;10(1):9613.
- Wang X, Dai Z, Wu X, Wang K, Wang X. Distinct RNA transcriptome patterns are potentially associated with angiogenesis in Tie2-expressing monocytes. *Gene.* 2016;580(1):1–7.
- Liang Z, Chi YJ, Lin GQ, Luo SH, Jiang QY, Chen YK. MiRNA-26a promotes angiogenesis in a rat model of cerebral infarction via PI3K/AKT and MAPK/ERK pathway. *Eur Rev Med Pharmacol Sci.* 2018;22(11):3485–92.
- Schober A, Nazari-Jahantigh M, Wei Y, Bidzhikov K, Gremse F, Grommes J, et al. MicroRNA-126-5p promotes endothelial proliferation and limits atherosclerosis by suppressing Dlk1. *Nat Med.* 2014;20(4):368–76.
- Esser JS, Saretzki E, Pankratz F, Engert B, Grundmann S, Bode C, et al. Bone morphogenetic protein 4 regulates microRNAs miR-494 and miR-126-5p in control of endothelial cell function in angiogenesis. *Thromb Haemost.* 2017;117(4):734–49.
- Huang JH, Xu Y, Yin XM, Lin FY. Exosomes derived from miR-126-modified MSCs promote angiogenesis and neurogenesis and attenuate apoptosis after spinal cord injury in rats. *Neuroscience.* 2020;424:133–45.
- Bidarimath M, Khalaj K, Kridli RT, Kan FW, Koti M, Tayade C. Extracellular vesicle mediated intercellular communication at the porcine maternal-fetal interface: a new paradigm for conceptus-endometrial cross-talk. *Sci Rep.* 2017;7:40476.

20. Wang Y, Lin X, Gong X, Wu L, Zhang J, Liu W, et al. Atypical GATA transcription factor TRPS1 represses gene expression by recruiting CHD4/NuRD(MTA2) and suppresses cell migration and invasion by repressing TP63 expression. *Oncogenesis*. 2018;7(12):96.
21. Serandour AA, Mohammed H, Miremadi A, Mulder KW, Carroll JS. TRPS1 regulates oestrogen receptor binding and histone acetylation at enhancers. *Oncogene*. 2018;37(39):5281–91.
22. Wilke CM, Hess J, Klymenko SV, Chumak VV, Zakhartseva LM, Bakhanova EV, et al. Expression of miRNA-26b-5p and its target TRPS1 is associated with radiation exposure in post-chernobyl breast cancer. *Int J Cancer*. 2018;142(3):573–83.
23. Hong J, Sun J, Huang T. Increased expression of TRPS1 affects tumor progression and correlates with patients' prognosis of colon cancer. *Biomed Res Int*. 2013;2013: 454085.
24. Wu M, Sun X, Wang T, Zhang M, Li P. TRPS1 knockdown inhibits angiogenic vascular mimicry in human triple negative breast cancer cells. *Clin Transl Oncol*. 2022;24(1):145–53.
25. Chen Y, Wang X. miRDB: an online database for prediction of functional microRNA targets. *Nucleic Acids Res*. 2020;48(D1):D127–31.
26. McGeary SE, Lin KS, Shi CY, Pham TM, Bisaria N, Kelley GM, et al. The biochemical basis of microRNA targeting efficacy. *Science*. 2019. <https://doi.org/10.1126/science.aav1741>.
27. Rauluseviute I, Riudavets-Puig R, Blanc-Mathieu R, Castro-Mondragon JA, Ferenc K, Kumar V, et al. JASPAR 2024: 20th anniversary of the open-access database of transcription factor binding profiles. *Nucleic Acids Res*. 2024;52(D1):D174–82.
28. Matsushima T, Inoue T, Suzuki SO, Fujii K, Fukui M, Hasuo K. Surgical treatment of moyamoya disease in pediatric patients—comparison between the results of indirect and direct revascularization procedures. *Neurosurgery*. 1992;31(3):401–5.
29. Hecht N, Marushima A, Nieminen M, Kremenetskaia I, von Degenfeld G, Woitzik J, et al. Myoblast-mediated gene therapy improves functional collateralization in chronic cerebral hypoperfusion. *Stroke*. 2015;46(1):203–11.
30. Anisimov A, Fang S, Hemanthakumar KA, Örd T, van Avondt K, Chevre R, et al. The angiopoietin receptor Tie2 is atheroprotective in arterial endothelium. *Nat Cardiovasc Res*. 2023;2(3):307–21.
31. He Q, Yuan R, Zhang T, An F, Wang N, Lan J, et al. Arabidopsis TIE1 and TIE2 transcriptional repressors dampen cytokinin response during root development. *Sci Adv*. 2022;8(36): eabn5057.
32. Nowicki M, Wierzbowska A, Małachowski R, Robak T, Grzybowski-Lzydorczyk O, Pluta A, et al. VEGF, ANGPT1, ANGPT2, and MMP-9 expression in the autologous hematopoietic stem cell transplantation and its impact on the time to engraftment. *Ann Hematol*. 2017;96(12):2103–12.
33. Zhao Y, Fu B, Chen P, Li Q, Ouyang Q, Zhang C, et al. Activated mesangial cells induce glomerular endothelial cells proliferation in rat anti-Thy-1 nephritis through VEGFA/VEGFR2 and Angpt2/Tie2 pathway. *Cell Prolif*. 2021;54(6): e13055.
34. Ma L, Brelen ME, Tsujikawa M, Chen H, Chu WK, Lai TY, et al. Identification of ANGPT2 as a new gene for neovascular age-related macular degeneration and polypoidal choroidal vasculopathy in the Chinese and Japanese populations. *Invest Ophthalmol Vis Sci*. 2017;58(2):1076–83.
35. Mao L, Wang Y, Wang D, Han G, Fu S, Wang J. TEMs but not DKK1 could serve as complementary biomarkers for AFP in diagnosing AFP-negative hepatocellular carcinoma. *PLoS ONE*. 2017;12(9): e0183880.
36. Han Q, Zhang Q, Ying F, Wang Z, Zhang Y, Gong L, et al. Circulating Tie2-expressing monocytes: a potential biomarker for cervical cancer. *Onco Targets Ther*. 2020;13:8877–85.
37. Xue R, Sheng Y, Duan X, Yang Y, Ma S, Xu J, et al. Tie2-expressing monocytes as a novel angiogenesis-related cellular biomarker for non-small cell lung cancer. *Int J Cancer*. 2021;148(6):1519–28.
38. Saharinen P, Eklund L, Miettinen J, Wirkkala R, Anisimov A, Winderlich M, et al. Angiopoietins assemble distinct Tie2 signalling complexes in endothelial cell-cell and cell-matrix contacts. *Nat Cell Biol*. 2008;10(5):527–37.
39. Karabid NM, Wiedemann T, Gulde S, Mohr H, Segaran RC, Geppert J, et al. Angpt2/Tie2 autostimulatory loop controls tumorigenesis. *EMBO Mol Med*. 2022;14(5): e14364.
40. Felcht M, Luck R, Schering A, Seidel P, Srivastava K, Hu J, et al. Angiopoietin-2 differentially regulates angiogenesis through TIE2 and integrin signaling. *J Clin Invest*. 2012;122(6):1991–2005.
41. Huang J, Zhu L, Qiu C, Xu X, Zhang L, Ding X, et al. MicroRNA miR-126-5p enhances the inflammatory responses of monocytes to lipopolysaccharide stimulation by suppressing cylindromatosis in chronic HIV-1 infection. *J Virol*. 2017. <https://doi.org/10.1128/JVI.02048-16>.
42. Haidar M, Rchiad Z, Ansari HR, Ben-Rached F, Tajeri S, Latre De Late P, et al. miR-126-5p by direct targeting of JNK-interacting protein-2 (JIP-2) plays a key role in Theileria-infected macrophage virulence. *PLoS Pathog*. 2018;14(3): e1006942.
43. Kavakiotis I, Alexiou A, Tastsoglou S, Vlachos IS, Hatzigeorgiou AG. DIANA-miTED: a microRNA tissue expression database. *Nucleic Acids Res*. 2022;50(D1):D1055–61.
44. Wang F, Li L, Sun X, Cai X, Wang J, Luo H, et al. The feedback loop between miR-222-3p and ZEB1 harnesses metastasis in renal cell carcinoma. *Cell Death Discov*. 2025;11(1):97.
45. Huang JZ, Chen M, Zeng M, Xu SH, Zou FY, Chen D, et al. Down-regulation of TRPS1 stimulates epithelial-mesenchymal transition and metastasis through repression of FOXA1. *J Pathol*. 2016;239(2):186–96.
46. Wang X, Zhu Q, Lin Y, Wu L, Wu X, Wang K, et al. Crosstalk between TEMs and endothelial cells modulates angiogenesis and metastasis via IGF1-IGF1R signalling in epithelial ovarian cancer. *Br J Cancer*. 2017;117(9):1371–82.
47. Ji J, Zhang G, Sun B, Yuan H, Huang Y, Zhang J, et al. The frequency of tumor-infiltrating Tie-2-expressing monocytes in renal cell carcinoma: its relationship to angiogenesis and progression. *Urology*. 2013;82(4):974.e9–13.
48. Wu X, Guan S, Lu Y, Xue J, Yu X, Zhang QI, et al. Macrophage-derived SHP-2 inhibits the metastasis of colorectal cancer via Tie2-PI3K signals. *Oncol Res*. 2023;31(2):125–39.
49. García S, Krausz S, Ambarus CA, Fernández BM, Hartkamp LM, van Es IE, et al. Tie2 signaling cooperates with TNF to promote the pro-inflammatory activation of human macrophages independently of macrophage functional phenotype. *PLoS ONE*. 2014;9(1): e82088.
50. Pucci F, Venneri MA, Bizziato D, Nonis A, Moi D, Sica A, et al. A distinguishing gene signature shared by tumor-infiltrating Tie2-expressing monocytes, blood “resident” monocytes, and embryonic macrophages suggests common functions and developmental relationships. *Blood*. 2009;114(4):901–14.
51. Coffelt SB, Chen YY, Muthana M, Welford AF, Tal AO, Scholz A, et al. Angiopoietin 2 stimulates TIE2-expressing monocytes to suppress T cell activation and to promote regulatory T cell expansion. *J Immunol*. 2011;186(7):4183–90.
52. Woś J, Chocholska S, Kowalska W, Tomczak W, Szymańska A, Karczmarczyk A, et al. Prognostic value of Tie2-expressing monocytes in chronic lymphocytic leukemia patients. *Cancers*. 2021;13(11):2817.
53. Jeong JH, Ojha U, Lee YM. Pathological angiogenesis and inflammation in tissues. *Arch Pharm Res*. 2021;44(1):1–15.
54. Zamora C, Cantó E, Vidal S. The dual role of platelets in the cardiovascular risk of chronic inflammation. *Front Immunol*. 2021;12: 625181.
55. Sainson RC, Johnston DA, Chu HC, Holderfield MT, Nakatsu MN, Crampton SP, et al. TNF primes endothelial cells for angiogenic sprouting by inducing a tip cell phenotype. *Blood*. 2008;111(10):4997–5007.
56. Zhuang PY, Wang JD, Tang ZH, Zhou XP, Quan ZW, Liu YB, et al. Higher proliferation of peritumoral endothelial cells to IL-6/sIL-6R than tumoral endothelial cells in hepatocellular carcinoma. *BMC Cancer*. 2015;15:830.
57. Zheng D, Liu J, Piao H, Zhu Z, Wei R, Liu K. ROS-triggered endothelial cell death mechanisms: focus on pyroptosis, parthanatos, and ferroptosis. *Front Immunol*. 2022;13:1039241.

Publisher's Note

Springer Nature remains neutral with regard to jurisdictional claims in published maps and institutional affiliations.